The Aluminum–Nitrogen Bond in Monomeric Bis(amino)alanes: A Systematic Experimental Study of Bis(tetramethylpiperidino)alanes and Quantum Mechanical Calculations on the Model System $(H_2N)_2AlY$

Klaus Knabel, Ingo Krossing[1], Heinrich Nöth*, Holger Schwenk-Kircher[2], Martin Schmidt-Amelunxen[2], and Thomas Seifert[2]

Institute of Inorganic Chemistry, University of Munich,
Meiserstraße 1, D-80333 Munich, Germany

Received November 10, 1997

Keywords: Aminoalanes / Alanes / Ab initio calculations / ^{27}Al-NMR spectroscopy / Structure elucidation / Substituent effects

Reactions of metallated nucleophiles M^IY [Y = OR, SR, NR_2, PR_2, AsR_2, CR_3, $Si(SiMe_3)_3$, R = organyl, H] with bis(2,2,6,6-tetramethylpiperidino)aluminum halides [tmp_2AlX, (X = Cl, Br, I)] offer facile access to a variety of bis(amino)alanes of the type tmp_2AlY. As indicated by ^{27}Al-NMR spectroscopy, mass spectrometry and X-ray crystal structure determinations, all of these compounds are monomeric in the solid state, in solution, and in the gas phase. Even Al–E single bonds (E = Si, P, As etc.) that are not commonly encountered are stabilized by the supporting tmp fragments. The results of a systematic analysis of the bonding parameters determined for the tmp_2AlY compounds, combined with a quantum mechanical study on model compounds $(H_2N)_2AlY$, not only reveal the presence of a highly polar Al–N bond, but at the same time rule out AlN-pp(π) bonding, in contrast to the situation in the analogous tmp_2BY compounds. It is shown that the Al–N bond length depends on the acidic character of the protic species HY: the shorter *d*(Al–N), the less basic is Y.

Introduction

Homo- and heteroatomic multiple bonding, especially involving heavier main-group elements, has been a major field of interest in the last decade. Thus, many compounds with element−element double bonds, kinetically stabilized by using bulky substituents attached to the element atom in question, have been produced. Application of this principle has led to the synthesis and characterization of Si=Si, Ge=Ge, Sn=Sn[3][4][5] and III−V (B=N, B=P, B=As)[6][7][8] doubly bonded systems. In the latter species, bond shortening and small twist angles between the planes at boron and the group-V elements are reported, indicative of pp(π) interactions. By means of variable-temperature ^{1}H-NMR spectroscopy[9] and quantum mechanical calculations[10], activation barriers for rotation about the B−E bond (E = N, P, As) as high as 33 kcal/mol have been determined.

Considering the heavier homologues of boron, i.e. aluminum and gallium, these might also be capable of adopting such bonding arrangements. However, no compounds containing Al=P or Al=As double bonds have yet been characterized. Thus, the gallyl phosphide $tBu_2GaP(Mes)(SiPh_3)$ exhibits a barrier to rotation about the Ga−P bond of only 12.7 kcal/mol[11]. Taking this result, together with an almost planar (sum of bond angles 346.2°) geometry at the phosphorus atom and a short Ga−P bond length, the authors concluded that a small pp(π) contribution might be present[11]. In the case of aluminum amides, pp(π) interaction, well established for the homologous aminoboranes[6][9], has been used to explain short bond lengths in monomeric aminoalanes {e.g. 1.78(2) Å in $Al[N(SiMe_3)_2]_3$ and 1.782(2) Å in $(MeAlNdipp)_3$ (dipp = 2,6-$iPr_2C_6H_3$)}[12][13]. Moreover, a barrier to rotation about the Al−N bond in $tBu_2AlN(dipp)(SiPh_3)$ of 9.9 kcal/mol has been determined, indicative of weak pp(π) interactions[14]. However, Al−N bond lengths in tricoordinated aluminum amides vary considerably from 1.78 to 1.88 Å. An analysis of structural data and rotational barriers in tricoordinated Al−N compounds lead to the conclusion that the bonding is primarily determined by Al−N bond polarity[15]. However, no systematic analysis on the variation of Al−N bonding parameters in a family of compounds has so far been performed. We found that bis(tetramethylpiperidino)alanes represent such a family.

Recently, we published the synthesis and structures of the monomeric bis(2,2,6,6-tetramethylpiperidino)aluminum halides {tmp_2AlX [X = Cl (**1a**), Br (**1b**), I (**1c**)]}[16], which allow even the synthesis of transition-metal compounds such as $[tmp_2Al-Fe(cp)(CO)_2,]$ (**2**)[17]. Here, we report on a variety of additional derivatives of bis(tmp)alanes. The compounds **1a−c**, **2**, and of the type tmp_2AlY **3−6** {Y = OR, SR, NR_2, PPh_2, $AsPh_2$, CR_3, $Si[Si(Me)_3]_3$, R = organyl, H} possess tricoordinated aluminum and nitrogen centers. To allow a distinction to be made between possible pp(π) interactions, N(p)AlX(σ*) interactions and a highly polar bonding situation at the aluminum center [χ(N) = 3.1; χ(Al) = 1.6; Pauling electronegativity], the structures of these compounds were determined in the solid state. Systematic variation of the group Y not only changes the electronic situation at the aluminum atom, but − since the am-

  1434−1948/98/0808−1095 $ 17.50+.50/0

ino ligands remain constant − this allows quantification of the effect of various substituents at the Al−N unit.

Although most of the tmp_2AlY compounds are sterically severely crowded, we expected to obtain supporting evidence from ab initio calculations (MP2/6-31+G*) on systematically varied model compounds $(H_2N)_2Al-Y$ (**7a−h**) [Y = Cl, OH, SH, NH_2, PH_2, CH_3, SiH_3, $Al(NH_2)_2$], including NBO analysis for interpretation of their bonding situation in the LMBO picture (= Lewis picture)[18].

Synthesis and Reactions

In order to delineate the effects of a systematic change of the group Y in tmp_2AlY, the following results describe tmp_2AlY compounds in which the substituent Y is varied across the main-group elements from right to left. All bis(tmp)alanes were obtained by the metathesis of tmp_2AlX (X = Cl, Br, I) with nucleophiles Y^-. The reactions proceeded well in aliphatic organic solvents. Monitoring of the reactions by ^{1}H-NMR spectroscopy indicated the exclusive formation of compounds tmp_2AlY (**3−6**). Competing reactions, which commonly hamper aluminum chemistry (e.g. dismutation leading to mixtures), were not observed.

(i) Main Group VI Nucleophiles

When mixtures of tmp_2AlX **1a−c** with the freshly prepared lithium compounds PhOLi, dippOLi, PhSLi, and *t*BuSLi were refluxed in *n*-hexane solution for about three hours, the monomeric bis(tmp)aluminum phenolates and thiolates $tmp_2Al-OPh$ **3a**, $tmp_2Al-Odipp$ **3b**, $tmp_2Al-SPh$ **3c**, and $tmp_2Al-StBu$ **3d** were obtained in 54−87% yield. The relatively weak nucleophilic character of the lithium aryloxides and thiolates necessitates heating in this case to make reaction times suitably short.

$$tmp_2AlX + LiY \xrightarrow[-LiX]{\text{n-hexane}} tmp_2AlY \quad (1)$$

X = Cl, Br, I Y = OPh **3a**, Odipp **3b**

Y = SPh **3c**, StBu **3d**

(ii) Main Group V Nucleophiles

Powdered LiN(H)R (R = *t*Bu, Ph) and $LiEPh_2$ (E = P, As) react with tmp_2AlX (**1a−c**) in *n*-hexane solution at ambient temperature to give $tmp_2Al-N(H)tBu$ (**4a**), $tmp_2Al-N(H)Ph$ (**4b**), $tmp_2Al-PPh_2$ (**4c**), and $tmp_2Al-AsPh_2$ (**4d**) in 42−65% yield. To verify the donor properties of the phosphorus atom in **4c**, one equivalent of AlI_3 was added to a solution of the compound in benzene. From the resulting solution, crystals separated on cooling, which proved to be the trimeric I_2AlPPh_2 (**4e**). The supernatant solution was found to contain tmp_2AlI (**1c**), which was characterized by its NMR spectra[15].

(iii) Main Group IV Nucleophiles

PhLi (Bu_2O solution), *n*BuLi (*n*-hexane solution), freshly prepared *p*-$MeOC_6H_4MgBr$ (THF), $H_{10}B_{10}C_2Li_2$ (= 1,2-dilithio-1,2-dicarba-*closo*-dodecaborane) and the tmeda adduct of $FecLi_2$ (Fec = ferrocene) each reacted smoothly with tmp_2AlX (**1a−c**) (within minutes to one hour) to give the organylalanes tmp_2Al-Ph (**5a**), tmp_2Al-Bu (**5b**), $tmp_2Al-C_6H_4OMe$ (**5c**), $(tmp_2Al)_2C_2B_{10}H_{10}$ (**5d**), and $(tmp_2Al)_2Fec$ (**5e**) in 48−79% yield. Reaction with $(Me_3Si)_3Si-Li(thf)_3$ afforded the silylalane $tmp_2Al-Si(SiMe_3)_3$ (**5f**) in 65% yield, whereas addition of freshly prepared $Me_3SnLi(thf)_x$ ($x \approx 3$) led only to the transient formation of $tmp_2Al-SnMe_3$ (**5g**), which quickly decomposed by stannylene elimination $(SnMe_2)_n$ to give tmp_2Al-Me (**5h**) as the sole isolated species. On leaving the latter compound to stand for several weeks in CO_2 at −78°C, quantitative insertion of CO_2 into the Al−N bonds occurred, resulting in the methylaluminum bis(carbaminate) $[MeAl(O_2Ctmp)_2]_2$ (**5i**).

The silylalane **5f** was subjected to a series of solvolysis reactions. Treatment with stoichiometric amounts of EtOH, PhOH, and HCl led exclusively to the products of Al−N cleavage $[(Me_3Si)_3SiAl(OEt)_2]_2$ (**5j**) and $[(Me_3Si)_3SiAlZ_3]tmpH_2$ [Z = OPh (**5k**), Cl (**5l**)] in 65−85% yield. Use of bulkier alcohols such as *t*BuOH, MesOH and dippOH led to inseparable mixtures, whereas 2,4,6-$tBu_3C_6H_2OH$ did not react.

$$tmp_2AlPPh_2 + AlI_3 \xrightarrow{\text{benzene}} [\,tmp_2AlPPh_2{*}AlI_3\,] \quad (2a)$$

4c

tmp_2AlI + $I_2Al(PPh_2)(AlI_2)PPh_2$

1c **4e**

(iv) Main Group III Nucleophiles

Suspensions of $LiBH_4$ or $Li(H_29\text{-BBN})$ (9-BBN = 9-borabicyclononane) in *n*-hexane reacted with tmp_2AlX compounds (X = Cl, Br, I) to afford the highly soluble compounds $tmp_2AlH_2BH_2$ (**6a**) (42%) and tmp_2AlH_2(9-BBN) (**6b**) (74%).

Characterization

Monomeric Bis(tmp)alanes

The chemical shift of the ^{27}Al-NMR signals of **1−6** is a function of the electron density at the aluminum nucleus (see Table 1). Strong σ- and possible π-donors such as the aryloxides, phosphanides, and arsanides **3a−b** and **4c−d** induce an upfield shift of the ^{27}Al signal up to δ = 65 [compared to tmp_2AlX (X = Cl, Br, I), $\delta^{27}Al = 130$][15]. Organyl or silyl substituents cause a deshielding, which reaches its maximum for $tmp_2Al-Si(SiMe_3)_3$ (**5f**) ($\delta^{27}Al = 186$). How-

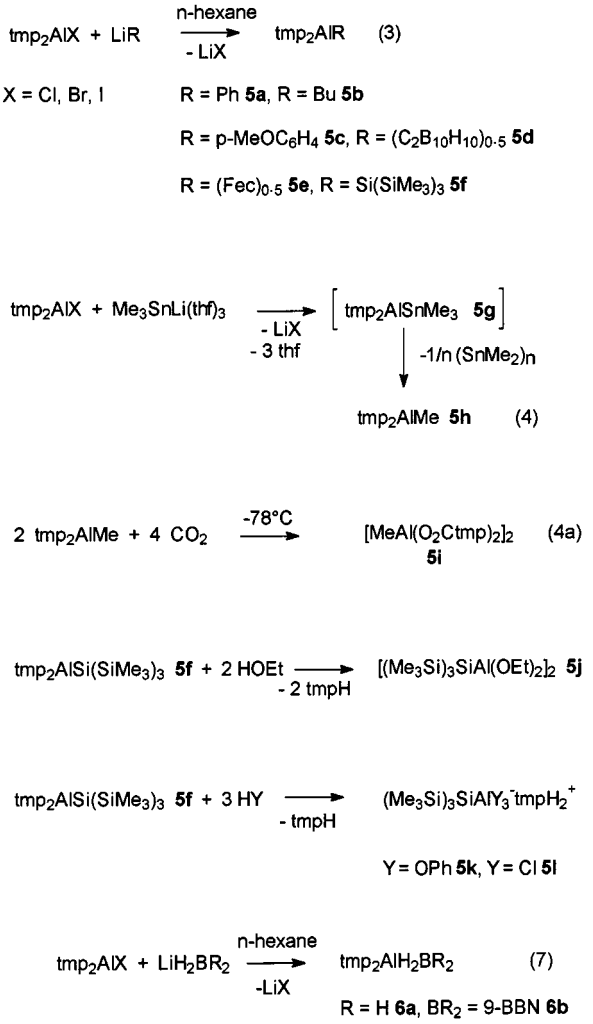

ever, there is one exception: δ^{27}Al of $(tmp_2Al)_2Fec$ (**5e**), possibly as a result of an anisotropic effect of the iron atom, exhibits a remarkable high-field shift (δ^{27}Al = 59). Due to the low local symmetry at the aluminum center, signals with half-widths as broad as 19400 Hz are a characteristic feature of the tricoordinated aminoalanes **2**−**6**[18][19]. The halides **1a**−**c** were shown to be monomeric by cryoscopic molar-mass determinations and, therefore, the signals in the ^{27}Al-NMR spectrum exhibit very broad half-widths of 9100−13700 Hz[15]. Since all other tmp_2AlY compounds possess the same local symmetry at the aluminum atom and exhibit signal half-widths similar to those observed in **1a**−**c**, it can be assumed that **2**−**6** do not form associates in solution.

In agreement with this assumption is the observation that in the ^{1}H- and ^{13}C-NMR spectra, only one set of resonances is observed for the tmp ligand, indicating free rotation about the Al−N bond and rapid inversion of the piperidinyl ring. In the case of the phosphanide **4c**, a long-range coupling [$^4J(^{31}P,^{13}C)$ = 4.1 Hz] of the tmp methyl carbon atoms and the phosphorus atom is characteristic. At ambient temperature, **5f**, probably the sterically most crowded molecule of this series, shows a set of broad ^{1}H-NMR and ^{13}C-NMR signals for the tmp methyl groups. Upon cooling to −70°C, these separate into two distinct lines (depicted in Figure 1). As the free activation enthalpy for this process has been determined to be about 54 kJ/mol (using the Eyring equation)[21], we take this as evidence for hindered inversion of the piperidinyl ring (cf. for example, the inversion barrier of cyclohexane: 46 kJ/mol)[22], while we assume free rotation about the Al−N bond even at a temperature of −70°C (if there was hindered rotation about the Al−N bond, one should observe four signals for the then magnetically inequivalent tmp methyl groups).

Table 1. Chemical shifts δ^{27}Al and line width of tmp_2 AlY compounds

tmp_2AlY compd.	**3a**	**3b**	**3c**	**3d**	**4a**	**4b**	**4c**	**4d**
R =	OPh	Odipp	SPh	S*t*Bu	N(H)*t*Bu	N(H)Ph	PPh_2	$AsPh_2$
δ^{27}Al[a]	75	85	153	152	129	124	110	74
$h_{1/2}$[b]	8800	9000	14000	9500	8700	9600	13400	18300

tmp_2AlY compd.	**5a**	**5b**	**5c**	**5d**	**5e**	**5f**	**5h**	**6b**
R =	Ph	Bu	[c]	[d]	$(Fec)_2$	$(Me_3Si)_3Si$	Me	H_29-BBN
δ^{27}Al[a]	153	164	160	164	59	186	173	115
$h_{1/2}$[b]	12300	13400	19400	12400	7400	12400	–	10700

[a] In ppm. − [b] In Hz. − [c] *p*-$MeOC_6H_4$.− [d] $(C_2B_{10}H_{10})_2$.

In the ^{11}B-NMR spectrum of the tetrahydroborate **6a** ($\delta^{11}B$ = −24.4), a $^1J(^{11}B,^1H)$ coupling constant of 85 Hz is found. This lies well within the range found for other aminoaluminum tetrahydroborates [e.g. $H_2B(\mu\text{-}NMe_2)\text{-}Al(BH_4)_2$, $^1J(^{11}B,^1H)$ = 89 Hz][23]. In contrast, the proton-coupled ^{11}B-NMR spectrum of **6b** exhibits only a broad, unresolved signal, which narrows on proton decoupling from 247 Hz to 207 Hz. From the IR spectra, a bidentate coordination of the BH_4 group to the aluminum atom can be deduced.

To investigate their gas-phase behavior, **3d**, **5a**−**b**, **h**, and **6a** were subjected to mass spectrometry (70 eV). No fragments of higher *m*/*z* ratios than the molecular ions of the monomers (15−20% relative intensity) were observed, confirming the unassociated nature of these species in the vapour phase. Due to the low Al−C and Al−H bond strengths[24], the bis(tmp)aluminum cation tmp_2Al^+, *m*/*z* = 307, is formed as the major fragment with 18−100% relative intensity. Since these compounds contain eight methyl groups, the (M − 15) fragment is formed very readily (31−100% relative intensity). It is noteworthy that the phosphanide **4c**, the arsanide **4d**, and the silylalane **5f** decomposed upon vaporization; only fragments of low *m*/*z* ratio were detected.

^{1}H- and ^{13}C-NMR spectroscopic analysis of the crystals and the supernatant solution obtained according to equation 2a revealed Al−P bond cleavage of the presumably formed adduct $tmp_2AlPPh_2{*}AlI_3$. The crystals only gave rise to signals in the aromatic region, while the solution

Figure 1. ^{1}H-NMR and ^{13}C-NMR spectra of **5f** in [D_8]toluene recorded at various temperatures

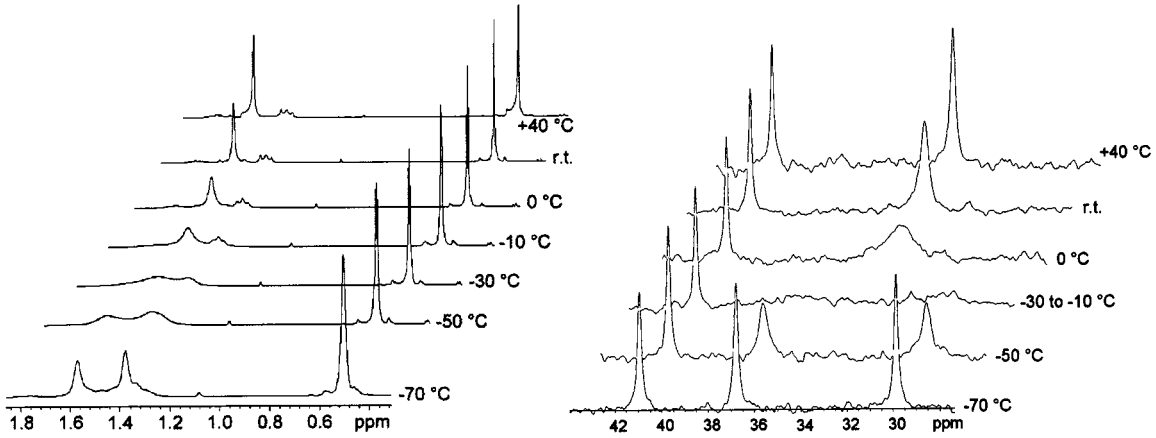

exhibited signals attributable to tmp_2AlI (**1c**)[15]. The ^{31}P-NMR signal of **4e** is shifted downfield compared to **4c**, appearing at $\delta^{31}P = -42.9$, thus indicating a tetracoordinated phosphorus atom. Since **4e** is trimeric in the solid state, as ascertained by X-ray crystal structure determination, it is most likely that the phosphanide retains this degree of oligomerization in solution. This would correspond to the behavior of $(Me_2AlPMe_2)_3$[25].

The ^{27}Al-NMR spectrum of the aluminum carbaminate **5i** shows two sharp signals in the region typical of pentacoordinated species [$d^{27}Al = 21$ ($\Delta_{1/2} = 1.120$ Hz); $d^{27}Al = 9$ ($\Delta_{1/2} = 980$ Hz)] {cf. $[(Me_2NCS_2)_2AlCl]_2$: $d^{27}Al = 14$}[26], indicating that the dimeric compound found in the solid state (vide infra) dissociates in solution partly into monomers . This is confirmed by ^{1}H- and ^{13}C-NMR spectroscopy. Two sets of signals are observed for the tmp ligands, those assigned to the dimer having twice the intensity (see Figure 2).

Figure 2. Possible bonding patterns of the carbaminate **5i**

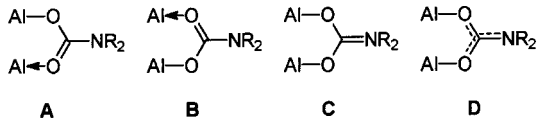

Considering the IR spectrum, formula **D** is consistent with the strong absorption at 1582 cm^{-1}. Thus, the partial C−N double bond, as indicated by the rather short C−N bond length (vide infra), results in hindered rotation about this bond and makes inversion of the ring more difficult, rendering pairs of atoms in the tmp ligand magnetically inequivalent.

The presence of tetracoordinated aluminum centers in the silylalane **5j** and the silylaluminates **5k−l** is evident from the dramatically decreased line widths in the ^{27}Al-NMR spectra ($\Delta_{1/2} = 1000-3000$ Hz vs. 12400 Hz in **5f**)[18]. A double set of lines for the ethoxy groups in **5j** indicates its dimeric nature (terminal and bridging EtO resonances) and rules out the possibility that a mixture of *cis* and *trans* isomers is present, since only one signal for the bridging ethoxy group is found. Most probably, the terminal EtO groups are oriented *trans* to one another, as this isomer crystallizes from the solution (the *trans* isomer is favoured by about 6 kcal/mol according to a semiempirical AM1 calculation). Aluminate formation in the case of **5k−l** is deduced from the ^{13}C-NMR signals of the $tmpH_2^+$ cation, which differ markedly compared to those observed when a tricoordinated nitrogen atom is present in the piperidino ligand [e.g. $\delta^{13}C$ (N−*C*) = 57−58 vs. 51−53 in tmp_2AlY], and from the presence of an NH_2 stretching band in the IR spectrum. The ^{29}Si-NMR signals of the $Me_3{}^{29}Si$ groups of **5j−l** fall in the small range of $\delta = -8$ to -10, well within the range of reported values for the homologous gallium compounds prepared by Linti et al.[27]. Compared to **5f**, the ^{1}H-NMR signals for the Me_3Si groups are shifted by 0.3−0.4 ppm to higher field. We attribute this to the reduced steric crowding that results from the replacement of the tmp ligands with less bulky substituents.

Crystal Structures

Monomeric Bis(tmp)alanes tmp_2AlY (3−6)

Structural parameters are presented in Table 2, additional values are given in the caption of each ORTEP representation. Hydrogen atoms are omitted for clarity in the figures except in the plots of **4b** and **6b** where selected hydrogen atoms are depicted. All molecules **3−6** possess tricoordinated aluminium atoms residing in a planar envirnonment [sum of bond angles $\Sigma(Al) = 360.0°$]. The nitrogen atoms of the tmp ligands, which exhibit the chair conformation, seem to have sp^2 character, as their sum of bond angles range from 359.4 to 360.0°.

$tmp_2AlOdipp$ (3b)

The structure of **3b** is depicted in Figure 3. The molecule shows a rather long Al−O distance of 1.696(2) A, compared to that in the electronically similar tris(aryloxides) [e.g. $Al(OAr)_3$, OAr = 2,6-tBu$_2$-4-Me-C_6H_2, d(Al−O) = 1.647 A (av.)][28] investigated by Barron et al. Due to the steric requirements of the bulky substituents, the Al−O−C angle, 158.4(2)°, is rather large a feature commonly observed for monomeric aluminum aryloxides. This can be

Table 2. Some characteristic bonding parameters of tmp_2AlY compounds

tmp_2AlY Y =	d(Al−N) [Å]	d(Al−E) [Å]	N−Al−N [°]	C−N1−Al−E [°]	C−N2−Al−E [°]	Σ(N) [°]	Σ(Al) [°]
Cl[a] (**1a**)	1.785(4)	2.144(2)	130.1(2)	66.2	30.8	357.6	360.0
	1.810(4)			84.3	52.1	356.7	
Br[a] (**1b**)	1.782(6)	2.309(2)	130.4(3)	66.0	31.1	357.5	359.8
	1.812(6)			88.7	46.9	356.9	
I[a] (**1c**)	1.788(3)	2.571(1)	129.5(1)	65.2	35.6	357.9	359.9
	1.803(3)			89.3	48.8	357.1	
Odipp (**3b**)	1.807(2)	1.696(2)	128.9(1)	59.5	57.4	359.8	360.0
	1.809(2)			59.4	62.7	360.0	
SPh (**3c**)	1.800(2)	2.225(1)	128.2(1)	−141.0	59.6	360.0	360.0
	1.807(2)			37.8	−106.9	358.9	
	1.798(2)	2.233(1)	130.8(1)	119.4	110.3	358.6	360.0
	1.813(2)			−44.1	−60.3	359.5	
S*t*Bu (**3d**)	1.817(2)	2.200(1)	128.6(1)	−73.5	−70.6	359.9	360.0
	1.820(2)			109.9	116.1	359.8	
N(H)Ph (**4b**)	1.813(2)	1.790(2)	131.8(1)	66.2	67.2	359.9	360.0
	1.822(2)			70.4	70.2	359.9	
PPh_2 (**4c**)	1.819(2)	2.377(1)	128.8(1)	65.3	65.1	359.9	360.0
	1.819(2)			66.7	68.7	360.0	
$AsPh_2$ (**4d**)	1.816(3)	2.485(2)	129.1(1)	65.5	64.9	359.9	360.0
	1.822(3)			69.6	66.1	360.0	
Ph (**5a**)	1.826(2)	1.971(3)	128.9(1)	67.7	−	359.8	359.9
				73.2			
$(Fec)_{0.5}$ (**5e**)	1.824(3)	1.952(3)	126.1(1)	69.7	61.6	359.8	360.0
	1.825(3)			74.0	62.0	359.9	
$(Me_3Si)_3Si$ (**5f**)	1.844(2)	2.514(1)	123.8(1)	76.5	59.9	359.6	360.0
	1.848(2)			82.9	66.8	359.6	
H_2(9-BBN)[d] (**6b**)	1.814(4)	2.223(7)	132.4(2)	67.1	−	359.4	360.0[d]
				75.9			
$Altmp_2$[b] (**8**)	1.849(1)	2.640(2)	121.8(1)	64.1	68.1	359.9	360.0
	1.851(2)			67.6	69.7	359.9	
$Fecp(CO)_2$ (**2**)[c]	1.847(4)	2.450(1)	121.9(2)	72.2	64.6	359.3	360.0
	1.862(4)			73.8	74.5	359.9	

[a] See ref.[15]. – [b] See ref.[49i]. – [c] See ref.[16]. – [d] Al···B distance.

taken as an indication of a strong polar Al−O bond, which should lead to a short Al−O bond[15].

tmp_2AlSPh (3c) (Figure 4) and $tmp_2AlStBu$ (3d) (Figure 5)

The asymmetric unit of **3c** contains two independent, slightly different molecules. Compared to the published structure of monomeric aluminum thiolates $(mes^*S)_3Al$ [mes* = 2,4,6-tBu$_3$C$_6$H$_2$, d(Al−S) = 2.185(2) Å][29], Bu-Al(Smes*)$_2$ [d(Al−S) = 2.188(9) Å] and tBuAl(Smes*)$_2$ [d(Al−S) = 2.196(3) Å][30], the Al−S distances found in **3c−d** are elongated [**3c**: 2.225(1), 2.233(1) Å; **3d**: 2.200(1) Å]. This is consistent with the lower basicity of PhS^- (compared to tBuS$^-$), since d(Al−S) in **3c** is longer, and d(Al−N) is shorter than in **3d**, and vice versa. The C−S−Al angles are 105.7(1)° and 106.5(1)° for **3c**, and 118.9(1)° for **3d** and, as expected, are smaller than the C−O−Al angles observed in **3b** [158.4(2)°] or $R_xAl(OAr)_{3-x}$ (R = organo, up to 171°)[27].

$tmp_2AlN(H)Ph$ (4b)

As the anilide **4b** (depicted in Figure 6) is the derivative of the primary amine $PhNH_2$, it belongs to the rare class of kinetically stabilized, hydrogen-bearing aluminum amides[15]. These are normally unstable with respect to intramolecular amine elimination and formation of oligomeric iminoalanes $(RAl-NR)_n$ (n = 2−8)[31][32]. The anilide

Figure 3. Molecular structure of $tmp_2AlOdipp$ (**3b**) in the solid state; thermal ellipsoids are shown at a 25% probability level[a]

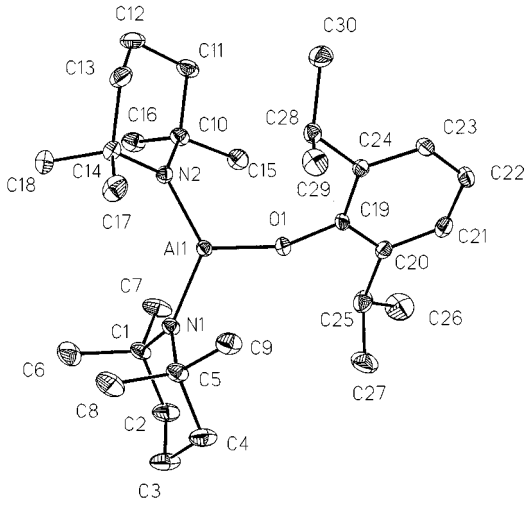

[a] Additional bond angles [°]: Al(1)−O(1)−C(19) 158.4(2), N(1)−Al(1)−O(1) 113.3(1), N(2)−Al(2)−O(1) 117.8(1).

Al−N bond [1.790(2) Å] is shorter than the Al−N bonds to the piperidino ligand [1.813(2) and 1.822(2) Å], presumably due to the reduced steric requirement of the ligand. However, in the monomeric tris(amides) $Al[N(SiMe_3)]_3$[12] and $Al(NiPr_2)_3$[33] similar or even shorter Al−N bond

Figure 4. Molecular structure of one of the two independent species of tmp_2AlSPh (**3c**) in the solid state; thermal ellipsoids are shown at a 25% probability level[a]

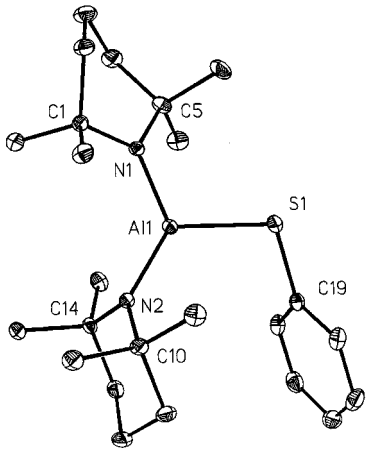

[a] Bond lengths [A] and bond angles [°]: Al(1)−S(1) 2.225(1), Al(2)−S(2) 2.233(1); C(19)−S(1)−Al(1) 105.7, C(43)−S(2)−Al(2) 106.5, N(1)−Al(1)−S(1) 110.1(1), N(2)−Al(1)−S(1) 121.7(1), N(3)−Al(2)−S(2) 109.4(1), N(4)−Al(2)−S(2) 119.6(1).

Figure 5. Molecular structure of $tmp_2AlStBu$ (**3d**) in the solid state; thermal ellipsoids are shown at a 25% probability level[a]

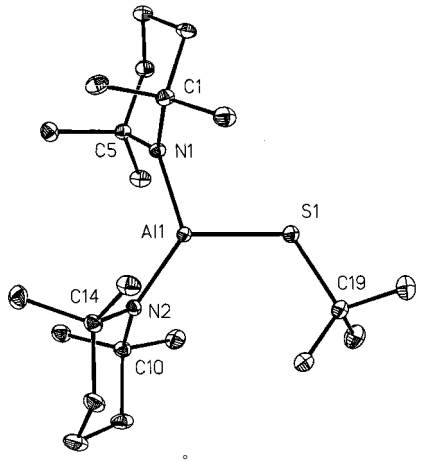

[a] Additional bond lengths [A] and bond angles [°]: Al(1)−S(1) 2.220(1); C(19)−S(1)−Al(1) 118.9(1), N(1)−Al(1)−S(1) 107.0(1), N(2)−Al(1)−S(1) 124.4(1).

lengths are reported [1.78(2) A for the silylamide and 1.791(4)−1.801(4) A for the isopropylamide]. The anilide N atom resides in a distorted trigonal-planar environment (sum of bond angles at the anilide nitrogen atom: 359.9°), with a large Al−N−C angle [138.9(2)°] and small Al−N−H and C−N−H angles [110.9(2) and 110.1(2)°].

tmp_2AlPPh_2 (4c) (Figure 7) and $tmp_2AlAsPh_2$ (4d) (Figure 8)

4c−d are isotypic. The most important structural parameter of these compounds is the Al−E bond length [E = P: 2.377(1) A; E = As: 2.485(2) A]. Only a few bonding parameters of this kind are known at the present time.[15] Compared to the recently published tricoordinated aluminum phosphanide $trip_2Al-P(Ada)(SiPh_3)$ [d(Al−P) = 2.342(2) A; trip = 2,4,6-iPr$_3$C$_6$H$_2$; Ada = adamantyl][34] and to the sum of the relevant covalent radii [1.25 A (Al) + 1.10 A (P) = 2.35 A][35], the Al−P bond in **4c** is elongated. The arsanide **4d** represents a acyclic compound featuring an aluminum−arsenic σ-bond, although two molecules, the trimeric (mes*Al−AsPh)$_3$ [d(Al−As) = 2.43 A][36] and the cp*$_3$Al$_3$As$_2$ cluster [d(Al−As) = 2.48 A][37], have previously been subjected to crystal structure analyses. The latter compound may be viewed as a subvalent species, and thus it is inappropriate to compare its Al−As bond length with that in **4d**. Considering the sum of the covalent radii [1.25 A (Al) + 1.21 A (As) = 2.46 A][33], the Al−As single bond in **4d** seems to be slightly lengthened. The phosphorus and arsenic atoms in **4c−d** reside in pyramidal environments [sum of bond angles: 316.2° (P) and 308.1° (As)]. Due to its position in the main-group V, the geometry at the arsenic atom is more pyramidalized than that at the phosphorus atom [cf. for example, the sum of bond angles in PCl_3 (300.9°) and $AsCl_3$ (296.1°)]. The pyramidal P and As atoms, as well as the geometric orientations of the EPh_2 fragments relative to the N_2Al planes, prevent the formation of Al−E pp(π) bonds.

Figure 6. Molecular structure of $tmp_2AlN(H)Ph$ (**4b**) in the solid state; thermal ellipsoids are shown at a 25% probability level[a]

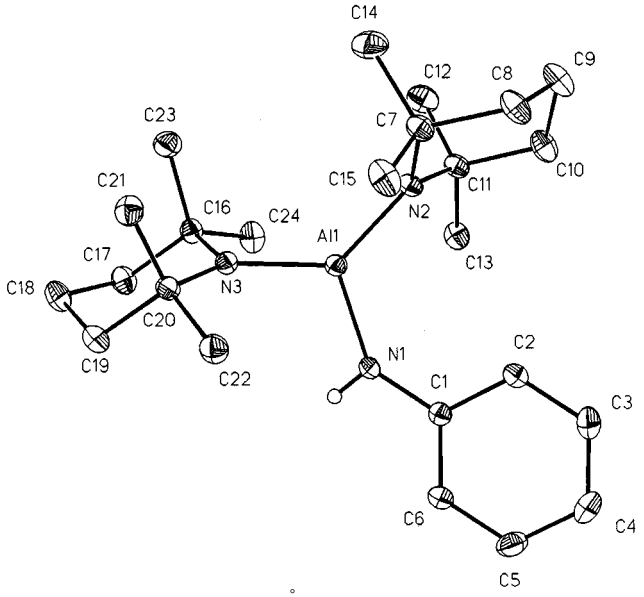

[a] Additional bond lengths [A] and bond angles [°]: Al(1)−N(1) 1.790(2); Al(1)−N(1)−C(1) 138.9(2), N(2)−Al(1)−N(1) 118.57(9), N(3)−Al(1)−N(1) 109.7(1), Al(1)−N(1)−H(1) 110.9(2), C(1)−N(1)−H(1) 110.1(2).

tmp_2AlPh (5a) (Figure 9) and $(tmp_2Al)_2Fec$ (5e) (Figure 10)

Colorless needles of **5a** are monoclinic, space group $C2/c$. There are four molecules in the unit cell, which suggests crystallographically imposed C_2 symmetry. The Al−C distances of 1.971(3) A (**5a**) and 1.952(3) A (**5e**) fall well within the range of published Al−C bond lengths for organylbis(amino)alanes [e.g. 1.970(3) A for Mes−Al[N(SiMe$_3$)$_2$]$_2$][15][38]. Due to the higher electronegativity of the ferrocenyl ligand, which is associated with more contracted orbitals, the Al−C bond in this compound is slightly shorter. The C−Al−N−C torsion angles are very

Figure 7. Molecular structure of tmp_2AlPPh_2 (**4c**) in the solid state; thermal ellipsoids are shown at a 25% probability level[a]

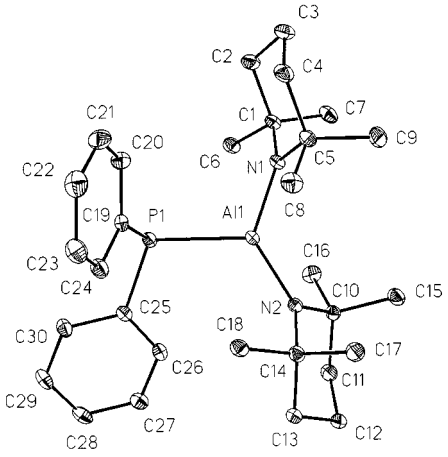

[a] Additional bond angles [°]: Al(1)−P(1) 2.377(1); Al(1)−P(1)−C(19) 100.55(8), Al(1)−P(1)−C(25) 110.90(9), N(1)−Al(1)−P(1) 109.35(7), N(2)−Al(1)−P(1) 121.76(7).

Figure 8. Molecular structure of $tmp_2AlAsPh_2$ (**4d**) in the solid state; thermal ellipsoids are shown at a 25% probability level[a]

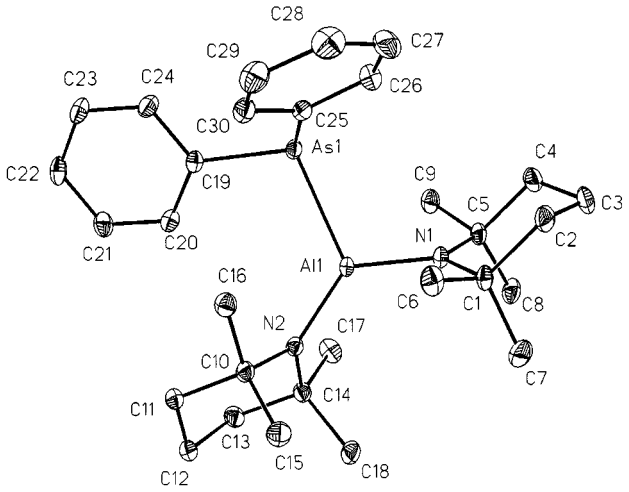

[a] Additional bond angles [°]: Al(1)−As(1) 2.485(2); Al(1)−As(1)−C(19) 108.3(1), Al(1)−As(1)−C(25) 97.6(1), N(1)−Al(1)−As(1) 108.8(1), N(2)−Al(1)−As(1) 122.1(1).

small (**5a**: 18.0°; **5e**: 7.2−15.8°), facilitating Al−C double bonding. However, closer examination of the reported Al−C distances in tetracoordinated alanes, which are not capable of bond shortening due to pp(π) interactions, is indicative of σ-bonding. Values of *d*(Al−C) similar to those in **5a** and **5e** are found in the tetracoordinated aminoalanes $(Me_2AlNC_6H_{12})_2$ [*d*(Al−C) = 1.963(6) and 1.986(7) A] and $(i\text{Bu}_2AlNMe_2)_2$ [*d*(Al−C) = 1.956(8) and 1.982(8) A][15][39]. In contrast to the crystal structures of the borylated ferrocenes $(Hal_2B)_nFec$ (Hal = Br, I; $n = 1-4$)[40], no Al−Fe interaction is apparent, which might have resulted from an interaction of the electron-deficient aluminum atom (with respect to an eight-electron system) and the electron-rich iron atom. The C−C−C−Al torsion angles of 12.5−12.9° reveal a bending of the $Altmp_2$ fragment away from the iron atom.

Figure 9. Molecular structure of tmp_2AlPh (**5a**) in the solid state; thermal ellipsoids are shown at a 25% probability level[a]

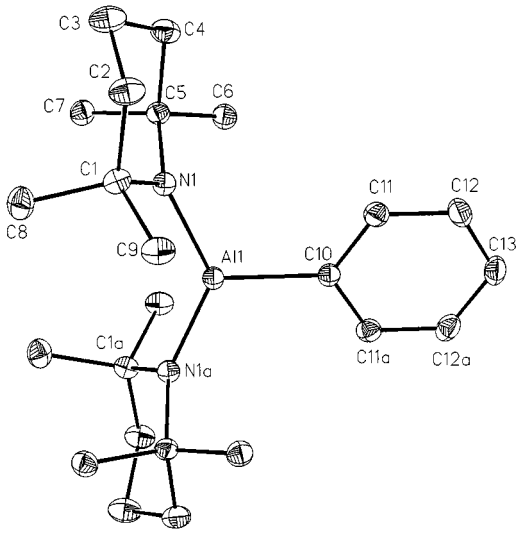

[a] Additional bond angles [°] and torsion angles [°]: Al(1)−C(10) 1.971(3); N(1)−Al(1)−C(10) 115.5(1); N(1)−Al(1)−C(10)−C(11) 18.0.

$tmp_2AlSi(SiMe_3)_3$ (5f)

The molecular structure of **5f** is depicted in Figure 11. Compared to a series of tetracoordinated silylalanes, which exhibit Al−Si distances of around 2.47 A[41], the bond length of 2.514(1) A found in **5f** is rather long, but is nevertheless in accordance with the steric demand of the ligands attached to the aluminum atom. Moreover, Linti et al. have prepared the homologous compound $tmp_2GaSi(SiMe_3)_3$, which, according to its crystal structure, exhibits the same structural features (e.g. long Ga−Si and Ga−N distances)[26] as **5f**. The decreased Si−Si−Si bond angles (av. 103.5°) may be attributable to steric factors, but could also be taken as an indication of a polar Al−Si bond (strong repulsion between the Al−Si σ-electrons and the Me_3Si groups due to the negative charge), since comparable angles have been found in the lithium silanides $(Me_3Si)_3SiLi^*(thf)_3$ and $(Me_3Si)_3SiLi(DME)_{1.5}$ (av. 102.4 and 104.0°)[42]. In the more relaxed $(Me_3Si)_3SiAlCl_3^-$, prepared by Stalke et al.[43], the Si−Si−Si bond angles are on average 110.0°.

$tmp_2AlH_2(9\text{-BBN})$ (6b)

6b forms colorless monoclinic crystals, space group *C*2/*c*, $Z = 4$ and possesses crystallographically imposed C_2 point group symmetry. The core of the structure consists of a four-membered AlH_2B ring. Since a twofold axis runs through Al1 and B1, this ring must be planar. The Al−H (1.738 A) and B−H (1.208 A) bond lengths are shorter than those found in aluminum tris(tetrahydroborate) $Al(BH_4)_3$ (1.80 A and 1.28 A). Moreover, *d*(Al−B) [2.223(7) A] is only 9 pm longer than the sum of their covalent radii (1.25 + 0.88 = 2.13 A)[33]. Assuming a bonding pattern as illustrated in Figure 13, the aluminum and boron atoms can be described as sp^2-hybridized, in accord with the large N−Al−N and C−B−C angles.

Figure 10. Molecular structure of $(tmp_2Al)_2Fec$ (**5e**) in the solid state; thermal ellipsoids are shown at a 25% probability level[a]

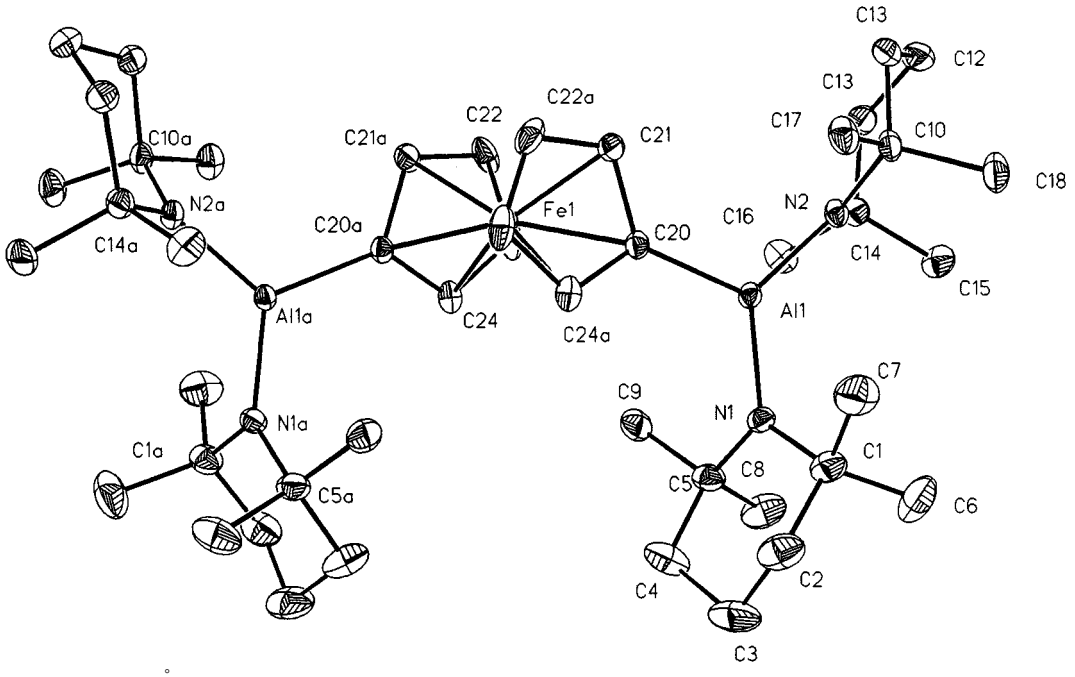

[a] Additional bond lengths [A] and bond angles [°] and torsion angles [°]: Al(1)−C(20) 1.952(3), Fe(1)−C(20) 2.103(3), Fe(1)−C(21) 2.036(3), Fe(1)−C(22) 2.028(3), Fe(1)−C(23) 2.049(3), Fe(1)−C(24) 2.065(3); N(1)−Al(1)−C(20) 117.4(1), N(2)−Al(1)−C(20) 116.1(1); C(21)−C(20)−Al(1)−N(2) 7.2, C(24A)−C(20)−Al(1)−N(1) 15.8.

Figure 11. Molecular structure of $tmp_2AlSi(SiMe_3)_3$ (**5f**) in the solid state; thermal ellipsoids are shown at a 25% probability level[a]

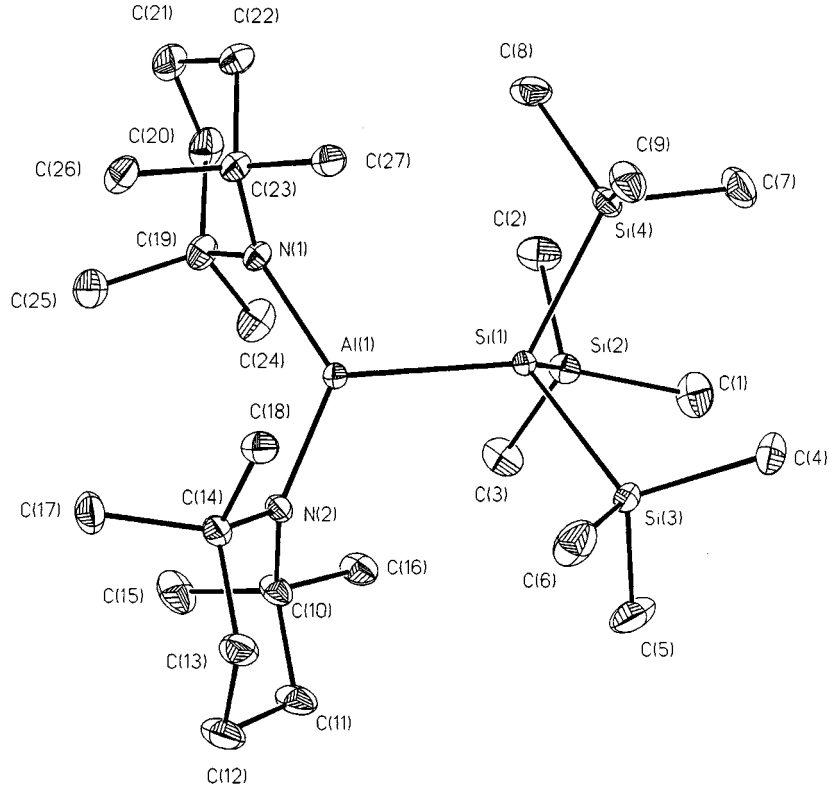

[a] Additional bond lengths [A] and bond angles [°]: Al(1)−Si(1) 2.5136(9), Si(1)−Si(2) 2.375(1), Si(1)−Si(3) 2.3703(9), Si(1)−Si(4) 2.3745(8); N(2)−Al(1)−Si(1) 117.81(6), N(1)−Al(1)−Si(1) 118.41(7), Si(3)−Si(1)−Al(1) 112.58(3), Si(4)−Si(1)−Al(1) 115.24(3), Si(3)−Si(1)−Si(4) 104.70(3), Si(3)−Si(1)−Si(2) 106.04(3), Si(4)−Si(1)−Si(2) 99.80(3), Si(2)−Si(1)−Al(1) 116.98(3).

Figure 12. Molecular structure of tmp_2AlH_2(9-BBN) (**6b**) in the solid state; thermal ellipsoids are shown at a 25% probability level[a]

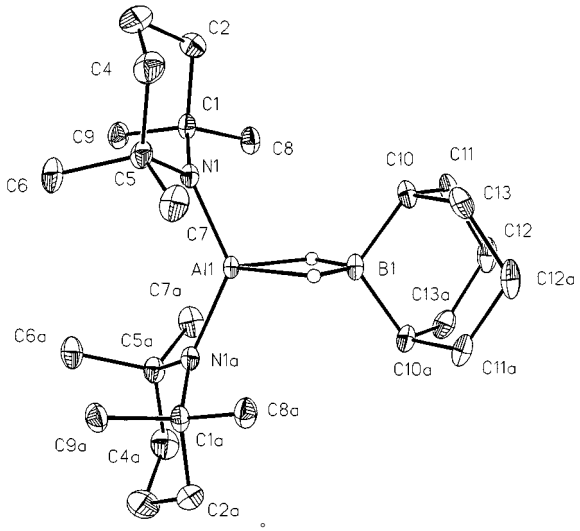

[a] Additional bond lengths [A] and bond angles [°]: Al(1)−B(1) 2.223(7), Al(1)−H(1) 1.738, B(1)−H(1) 1.208; N(1)−Al(1)−B(1) 113.8(1), H(1)−Al(1)−H(1A) 65.4, Al(1)−H(1)−B(1) 96.3, H(1)−B(1)−H(1A) 112.4.

Figure 13. Possible bonding pattern in **6b**

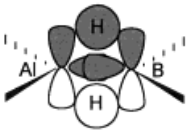

Whereas the N−Al−N angle in **6b** is as wide as 132.4°, and thus exceeds the 120° ideal by 12.4°, the C−B−C angle is only 110.2(6)°. Thus, the description of the bonding in **6b** is reminiscent of that of diborane[42]. A large exocyclic H−B−H angle of 121.8° and a short B−B distance of 1.71 A have been reported for this compound[42].

$(Ph_2PAlI_2)_3$ (4e)

Colorless prisms of **4e** crystallize in the trigonal space group $R\bar{3}$ with $Z = 24$ monomeric units. The six-membered ring is present in a chair conformation, (see Figure 14). The environment around each of the tetracoordinated Al and P atoms can be described as distorted tetrahedral, with maximum deviations of −8.2°/+4.6° from 109.5°. Values of d(Al−P) vary only slightly within the range from 2.435(2) to 2.461(3) A, and thus are very similar to the structural data of the trimeric phosphanylalane $(Me_2PAlMe_2)_3$ [d(Al−P) = 2.434(3) A], as determined by an electron diffraction study[24]. In contrast, the Al−P−Al [131.7(8)°] and P−Al−P [96.4(7)°] angles in $(Me_2PAlMe_2)_3$ differ considerably from those found in **4e** [114.8(1)−115.6(1)° and 108.2(1)−110.3(1)°]. Due to steric effects and bond polarity ($Al^{\delta+}-P^{\delta-}$), the Al−P−Al angles are widened compared to those in the cyclohexane ring. A siimilar behavior is observed in the homologous aminoalane trimers: Whereas in $(H_2Al-NMe_2)_3$ the Al−N−Al and N−Al−N angles are 114.9 and 108.8°, in $[Me_2Al-N(H)Me]_3$ these angles are 122.3 and 102.1°, respectively[24]. There is only a slight variation in the distance d(Al−I), the average being 2.532(2) A, which is in good agreement with the Schomaker-Stevenson corrected sum of the relevant sum of covalent radii (2.51 A)[33]. Moreover, for the compound $I_4Al_4(\mu\text{-}S)_2(\mu\text{-}SMe)_4$, which crystallizes in an adamantane-like Al_4S_6 framework bearing terminal iodine atoms, a similar bond length of 2.50 A has been reported[46].

Figure 14. Molecular structure of **4e** in the solid state; thermal ellipsoids are shown at a 25% probability level[a]

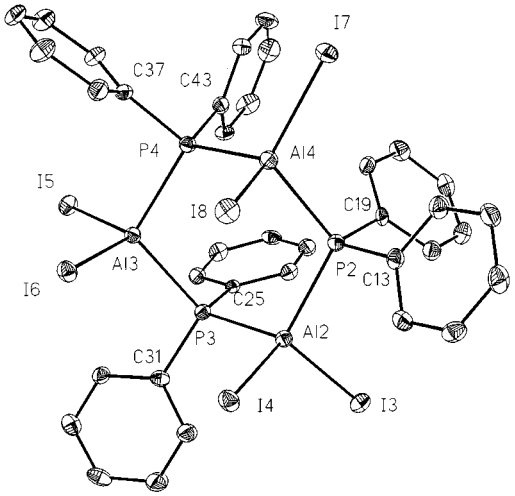

[a] Selected bond lengths [A] and bond angles [°]: Al(2)−P(2) 2.470(3), Al(2)−P(3) 2.461(3), Al(2)−I(3) 2.538(2), Al(2)−I(4) 2.541(2), Al(3)−P(3) 2.452(3), Al(3)−P(4) 2.438(3), Al(3)−I(5) 2.544(2), Al(3)−I(6) 2.525(2), Al(4)−P(4) 2.461(3), Al(4)−P(2) 2.444(3), Al(4)−I(7) 2.536(2), Al(4)−I(8) 2.521(2); Al(2)−P(3)−Al(3) 115.1(1), P(3)−Al(3)−P(4) 110.3(1), Al(3)−P(4)−Al(4) 114.8(1), P(4)−Al(4)−P(2) 108.2(1), Al(4)−P(2)−Al(2) 115.5(1), P(2)−Al(2)−P(3) 109.1(1), I(3)−Al(2)−I(4) 111.15(8), I(5)−Al(3)−I(6) 111.00(8), I(7)−Al(4)−I(8) 112.81(9).

$[MeAl(O_2Ctmp)_2]_2$ (5i)

Crystals of **5i** are very sensitive to warming and disintegrate when exposed to temperatures above −10°C (possibly due to a change of the modification?). The low-temperature phase is found to be monoclinic, space group $P2_1/c$, and contains two molecules in the unit cell (see Figure 15). The skeleton of **5i** is formed by two orthogonally linked, planar, eight-membered $C_2Al_2O_4$ rings, which meet at the pentacoordinated aluminum atoms. A C_4 axis (neglecting the Al−Me hydrogen atoms) passes through the Me−Al−Al−Me vector. The aluminum atoms reside in the center of a tetragonal pyramid, of which the four oxygen atoms form the base. The Al−Me groups are coordinated in an *exo* fashion, with short Al−C distances of 1.952(4) A to the pentacoordinated aluminum center. Longer Al−C bond lengths, up to 1.974(5) and 1.981(5) A, have been found for $\{AlMe_2[N(H)CH_2\text{-}2\text{-}Py]\}_2$[47]. The short Al−C bond in **5i** is due to the coordination of the Al center to four strongly electronegative oxygen atoms, which induce a positive charge at the Al atoms center, thereby reducing its effective radius due to coulombic interactions. The C30/31−N distances are consistent with a partial pp(π) double bond [d(C30/31−N) = 1.355(5) and 1.358(5) A]; the planes

through C_3N stand almost coplanar with those formed by the eight-membered rings. As indicated by the C−N−C−O torsion angles of 6.2 to 12.8°, C30 and C31 reside in planar environments, the O−C−O and N−C−O angles showing only very slight deviation from the 120° ideal (+/−0.5°). Coordination of the oxygen atoms to the aluminum nuclei is electrostatic, since the C−O−Al angles are found to be 133.4(3) to 136.4(3)°, and not of 115°, as would be expected for the appropriate hybridization of the oxygen atoms (intermediate between sp^2 and sp^3). In accordance with this description are quite long Al−O bonds, found in the range of 1.863(3) to 1.880(3) A, which adhere to the steric requirements of the carbaminate ligands.

Figure 15. Molecular structure of **5i** in the solid state; thermal ellipsoids are shown at a 25% probability level[a]

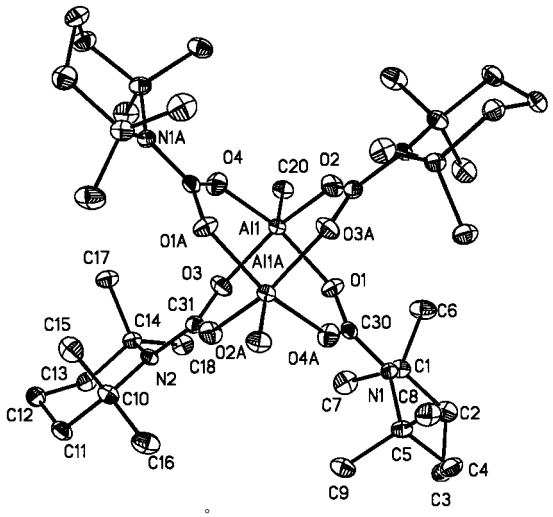

[a] Selected bond lengths [A] and bond angles [°] and torsion angles [°]: Al(1)−O(2) 1.863(3), Al(1)−O(3) 1.866(3), Al(1)−O(1) 1.873(3), Al(1)−O(4) 1.880(3), Al(1)−C(20) 1.952(4), O(1)−C(30) 1.271(5), O(2)−C(31A) 1.273(5), O(3)−C(31) 1.279(5), O(4)−C(30A) 1.270(4), N(1)−C(30) 1.358(5), N(1)−C(1) 1.524(5), N(1)−C(5) 1.527(4), N(2)−C(31) 1.355(5), N(2)−C(14) 1.516(5), N(2)−C(10) 1.520(4); O(2)−Al(1)−O(3) 149.2(1), O(2)−Al(1)−O(1) 85.6(1), O(3)−Al(1)−O(1) 86.1(1), O(2)−Al(1)−O(4) 86.3(13), O(3)−Al(1)−O(4) 86.0(1), O(1)−Al(1)−O(4) 149.4(1), O(2)−Al(1)−C(20) 105.3(2), O(3)−Al(1)−C(20) 105.5(2), O(1)−Al(1)−C(20) 105.1(2), O(4)−Al(1)−C(20) 105.5(2), C(30)−O(1)−Al(1) 133.4(3), C(31A)−O(2)−Al(1) 136.4(3), C(31)−O(3)−Al(1) 133.7(3), C(30A)−O(4)−Al(1) 136.1(3), C(30)−N(1)−C(1) 117.3(3), C(30)−N(1)−C(5) 117.2(3), C(1)−N(1)−C(5) 121.6(3), C(31)−N(2)−C(14) 117.1(3), C(31)−N(2)−C(10) 116.5(3), C(14)−N(2)−C(10) 123.4(3), O(4A)−C(30)−O(1) 120.8(3), O(4A)−C(30)−N(1) 119.7(3), O(1)−C(30)−N(1) 119.5(3), O(2A)−C(31)−O(3) 120.2(3), O(2A)−C(31)−N(2) 120.2(3), O(3)−C(31)−N(2) 119.7(3); C(5)−N(1)−C(30)−O(4A) 10.12, C(1)−N(1)−C(30)−O(1) 12.48, C(14A)−N(2A)−C(31A)−O(3A) 6.24, C(10A)−N(2A)−C(31A)−O(2) 12.82.

$[(Me_3Si)_3SiAl(OEt)_2]_2$ (5j)

The silylalane **5j** crystallizes in the monoclinic space group $P2_1/c$, with $Z = 2$ (see Figure 16). The central structural feature is, therefore, a four-membered, planar and crystallographically centrosymmetric Al_2O_2 ring [*d*(Al−O) = 1.833(4) A, O−Al−O = 80.7(2)°] with $(Me_3Si)_3Si$ and OEt ligands in *trans* positions. This is reminiscent of the recently published structure of $[tmp(Br)AlOEt]_2$, where these parameters are 1.827(6) A and 81.3(2)°, respectively[15]. The terminal Al−O distance [1.676(6) A] in **5j**, about 16 pm shorter than that of the Al−O bridge, is very similar to that found in $[H(OtBu)AlOtBu]_2$ [1.675(3) A][47]. The distance *d*(Al−Si) [2.444(2) A] is about 6 pm shorter than that in the starting material **5f** and other tetracoordinated silylalanes which show an average Al−Si distance of 2.47 A[39]. This lies at the lower end of the range of known Al−Si bond lengths, and indicates a relaxation in the steric strain on going from the tmp ligands to the EtO groups. Moreover, short Si−Si distances (2 pm shorter than that in **5f**) and acute Al−Si−Si angles are observed, which deviate up to 4.0° from the ideal angle of 109.5° (7.5° in **5f**).

Figure 16. Molecular structure of **5j** in the solid state; thermal ellipsoids are shown at a 25% probability level[a]

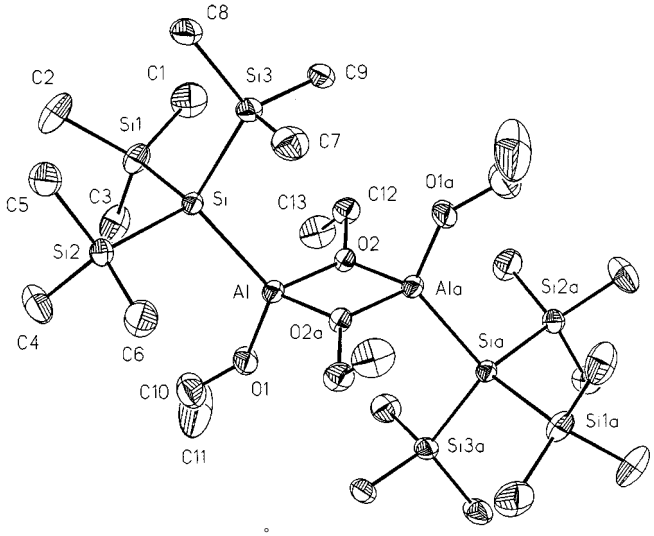

[a] Selected bond lengths [A] and bond angles [°]: Al−Si 2.444(2), Al−O(2A) 1.833(4), Al−O(1) 1.676(6), Al−O(2) 1.836(4), O(2)−Al(A) 1.833(4), Al−Al(A) 2.797(3), Si−Si(1) 2.350(2), Si−Si(2) 2.353(2), Si−Si(3) 2.353(2); O(1)−Al−O(2A) 106.0(2), O(1)−Al−O(2) 110.2(2), O(2A)−Al−O(2) 80.7 (2), O(1)−Al−Si 120.1(2), O(2)−Al−Si 115.3(1), Al(A)−O(2)−Al 99.3(2), Si(1)−Si−Si(3) 109.08(9), Si(3)−Si−Si(2) 107.94(9), Si(1)−Si−Si(2) 106.01(9), Si(3)−Si−Al 110.62 (8), Si(2)−Si−Al 109.86(8), Si(1)−Si−Al 113.11(9).

$[(Me_3Si)_3SiAl(OPh)_3]tmpH_2$ (5k) and $[(Me_3Si)_3SiAlCl_3]tmpH_2$ (5l)

Crystals of the triphenoxyaluminate **5h** are found to be monoclinic, space group $P2_1/n$. However, **5l** forms mixed crystals with $[tmpH_2]Cl$, a by-product of the reaction, without intermolecular contacts between the two species. Thus, the composition of compound **5l** corresponds to $[(Me_3Si)_3SiAlCl_3]tmpH_2*[tmpH_2]Cl$. The crystals are of the monoclinic space group $P2_1/c$, $Z = 4$. The aluminum atoms in **5k**, **l** reside in the centers of "tetrahedra" formed by three oxygen or chlorine atoms and one silicon atom (see Figures 17 and 18). Due to the steric demand of the phenoxy group, the angles in **5k** show larger deviation from the ideal value of 109.5° [97.4(1) to 117.1(1)°] than those in the trichloro derivative **5l** [104.7(1) to 113.0(1)°]. Both aluminate anions are linked to the $tmpH_2^+$ cations by hydrogen bonds. Whereas the triphenoxyaluminate **5k** forms two hydrogen

bonds to oxygen atoms incorporated in a six-membered, almost planar AlO_2H_2N ring, only one chlorine atom is coordinated by a hydrogen bond in **5l**. These atoms exhibit longer bond lengths to the aluminum center than their non-coordinated counterparts [**5k**: *d*(Al−O) = 1.775(3), 1.784(3) A vs. 1.736(3) A; **5l**: *d*(Al−Cl) = 2.187(3) A vs. 2.160(3), 2.166(3) A]. While the Al−Si distance in **5k** [2.468(3) A] corresponds to the average value[39] of 2.47 A, in the trichloro derivative **5l** it is only 2.420(3) A, which is even shorter than the Al−Si bond length found in the very similar compound $[(Me_3Si)_3SiAlCl_3]Li(thf)_4$ [2.446(1) A][41].

Figure 17. Molecular structure of **5k** in the solid state; thermal ellipsoids are shown at a 25% probability level[a]

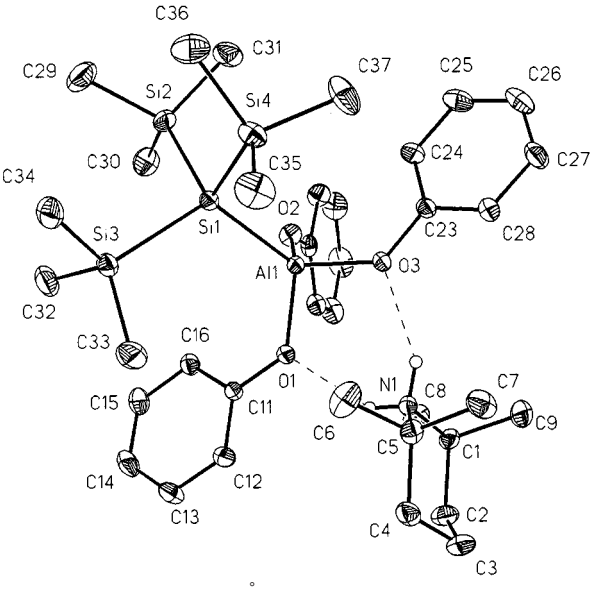

[a] Selected bond lengths [A] and bond angles [°]: Al(1)−O(1) 1.775(3), Al(1)−O(2) 1.736(3), Al(1)−O(3) 1.784(3), Al(1)−Si(1) 2.468(3), Si(1)−Si(2) 2.344(3), Si(1)−Si(3) 2.359(3), Si(1)−Si(4) 2.346(4); O(2)−Al(1)−O(1) 112.2(1), O(2)−Al(1)−O(3) 109.4(1), O(1)−Al(1)−O(3) 97.4(1), O(2)−Al(1)−Si(1) 107.2(1), O(1)−Al(1)−Si(1) 113.6(1), O(3)−Al(1)−Si(1) 117.1(1), Si(2)−Si(1)−Si(4) 106.6(1), Si(2)−Si(1)−Si(3) 104.24(9), Si(4)−Si(1)−Si(3) 105.41(9), Si(2)−Si(1)−Al(1) 107.0(1), Si(4)−Si(1)−Al(1) 115.2(1), Si(3)−Si(1)−Al(1) 117.4(1).

Al−N Bond Lengths and Related Structural Parameters

Although in the tricoordinated tmp_2AlY species **1−6** the tmp ligand is not changed, and thus little influence on *d*(Al−N) can therefore be expected, the observed Al−N bond lengths nevertheless vary from 1.782(6) to 1.862(4) A (see Table 2). These values are close to the shortest and longest Al−N distances reported for tricoordinated aminoalanes [e.g. 1.78(2) A for $Al[N(SiMe_3)_2]_3$, 1.782(4) A for $(MeAlNdipp)_3$, (dipp = 2,6-*i*Pr_2-C_6H_3) and 1.880(4) A for $tBu_2AlN(SiPh_3)_2$][12][13][14]. Moreover, an elongation of the Al−N bonds is observed when the ligand Y is varied from main-group VII (strongly electronegative ligands) to main-group III (electropositive ligands), reaching maximum values in the dialane(4)[48] [1.851(2) A] and the ferrioalane[16] [1.862(4) A]. An analysis of the structural parameters reveal a relationship between the N−Al−N bond angle and the Al−N bond lengths. For short Al−N bonds, a wide angle (> 130°) is noted, whereas compounds with long Al−N bonds exhibit smaller angles [down to 121.8(1)°]. This relationship cannot be associated with the steric effect of the attached ligands, since the sterically crowded aryloxide $tmp_2AlOdipp$ (**3b**) shows a large angle of 128.9(1)°, while the undemanding substituted ferrioalane **2** has a value of only 121.9(2)°. The orientation of perpendiculars through the nitrogen atoms in relation to the respective aluminum atoms indicates a strongly twisted orientation of the tmp ligands, with the relevant C−N−Al−E torsion angles (E = element) in **2−6** lying in the range of 57.4−82.9°.

Figure 18. Molecular structure of **5l** in the solid state; thermal ellipsoids are shown at a 25% probability level[a]

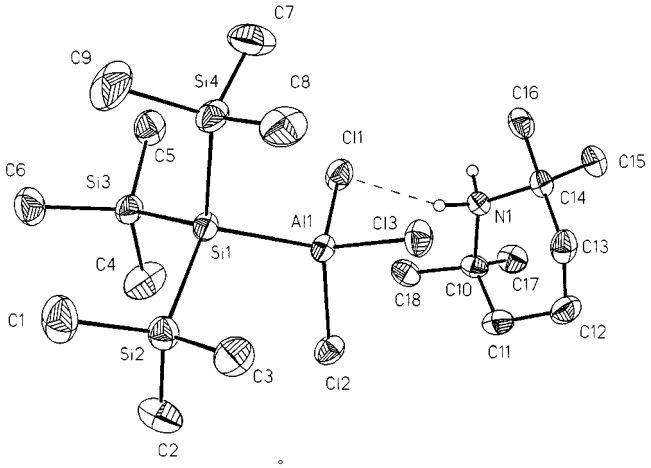

[a] Selected bond lengths [A] and bond angles [°]: Al(1)−Cl(3) 2.160(2), Al(1)−Cl(1) 2.187(3), Si(1)−Si(4) 2.331(3), Si(1)−Si(3) 2.342(3), Al(1)−Cl(2) 2.166(3), Al(1)−Si(1) 2.420(3), Si(1)−Si(2) 2.340(3), Si(2)−C(2) 1.858(5); Cl(3)−Al(1)−Cl(2) 106.48(7), Cl(2)−Al(1)−Cl(1) 104.66(1), Cl(2)−Al(1)−Si(1) 112.99(6), Si(4)−Si(1)−Si(2) 109.8(1), Si(2)−Si(1)−Si(3) 109.88(9), Si(2)−Si(1)−Al(1) 110.87(6), Cl(3)−Al(1)−Cl(1) 105.7(1), Cl(3)−Al(1)−Si(1) 115.5(1), Cl(1)−Al(1)−Si(1) 110.62(6), Si(4)−Si(1)−Si(3) 111.28(7), Si(4)−Si(1)−Al(1) 108.03(6), Si(3)−Si(1)−Al(1) 106.9(1).

Ab Initio Calculations of Model Compounds $(H_2N)_2AlY$

To gain an insight into the relationship between *d*(Al−N) and the N−Al−N bond angle, a series of ab initio calculations (MP2/6-31+G*)[17] has been performed on model compounds $(H_2N)_2AlY$, in which Y is systematically varied [Y = Cl (**7a**), OH (**7b**), SH (**7c**), NH_2 (**7d**), PH_2 (**7e**), CH_3 (**7f**), SiH_3 (**7g**), $Al(NH_2)_2$ (**7h**)]. The 6-31+G* basis set was chosen in order to provide a better approximation for the nitrogen lone pair and of the potentially highly polar Al−N bond. In this basis set, diffuse functions are implemented, which adequately describe electron density even far away from the nuclei. The structural parameters of the minimum structures are given in Table 3.

To understand the bonding situation in **7a−h**, natural bonding orbital analyses (NBO analyses) have been performed on the minimum energy structures. The results are listed in Table 3, and will be discussed later. It is apparent that the results of the calculations for the model compounds **7a−h** show the same trends as those observed in the crystal structures of **1−6**. The shortest Al−N bonds (1.782 A), are

Table 3. Calculated bonding parameters for bis(amino)alanes $(H_2N)_2AlY$ in their most stable configuration

Compound[a]	Sym.	d(Al−N) [A]	d(Al−E) [A]	N−Al−N [°]	q(Al) [e]	q(N) [e]	q(E) [e]	B.O. Al−N	LP[b] (Al)
$(H_2N)_2Al-Cl$ (**7a**)	C_{2v}	1.782	2.100	123.18	1.96	−1.53	−0.59	0.56	0.19
$(H_2N)_2Al-OH$ (**7b**)	C_s	1.786, 1.793	1.730	121.39	2.15	−1.54	−1.27	0.54, 0.55	0.17
$(H_2N)_2Al-SH$ (**7c**)	C_s	1.788, 1.791	2.192	121.39	1.89	−1.53	−0.66	0.55, 0.55	0.21
$(H_2N)_2Al-NH_2$ (**7d**)	D_{3h}	1.796	−	120.00	2.10	−1.53	−	0.53	0.19
$(H_2N)_2Al-PH_2$ (**7e**)	C_s	1.794	2.331	119.82	1.79	−1.53	−0.38	0.55	0.18
$(H_2N)_2Al-CH_3$ (**7f**)	C_s	1.799	1.962	117.91	2.00	−1.52	−1.33	0.54	0.15
$(H_2N)_2Al-SiH_3$ (**7g**)	C_s	1.797	2.451	119.09	1.67	−1.53	0.27	0.55	0.16
$(H_2N)_2Al-Al(NH_2)_2$ (**7h**)	D_2	1.804	2.579	116.71	1.40	−1.53	−	0.54	0.16

[a] All calculations MP2/6-31+G*.– [b] Number of electrons in $3p_z$ orbital of Al.

observed for the chloride **7a** and the longest for the dialane(4) **7h** (1.804 A); there is an inverse proportionality of d(Al−N) and the bond angle N−Al−N (large angles associated with short bond lengths). Moreover, the calculated Al−E bond lengths are in good agreement with the experimental values. Comparison with the crystal structures reveals that the observed correlation is not due to the steric requirements of the substituents, but is a consequence of the electronic situation (see Tables 2 and 3).

Discussion of Al−N Bonding

First of all, there is the paradox of the Al−N bonds: the shortest distances d(Al−N) ever found have been reported for compounds with tetracoordinated aluminum atoms [e.g. 1.767(3)−1.771(3) A in **9a**, 1.770(1) A in **9b**][49][50]. Therefore, the reason for the short bonds cannot be due to Al−N pp(π) interaction.

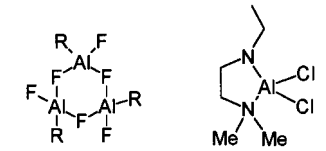

As all monomeric aminoalanes tmp_2AlX (**1**−**6**) contain planar tricoordinated nitrogen atoms in the tmp ligands, three Al−N bonding patterns (depicted in Figure 19) are possible to explain the trends in the Al−N bond lengths, namely pp(π) interaction (**D**), N(p)AlX(σ*) interaction (**E**), or a highly polar bonding situation (**F**).

Figure 19. Possible Al−N bonding patterns for the monomeric tmp_2AlY species **1**−**6**

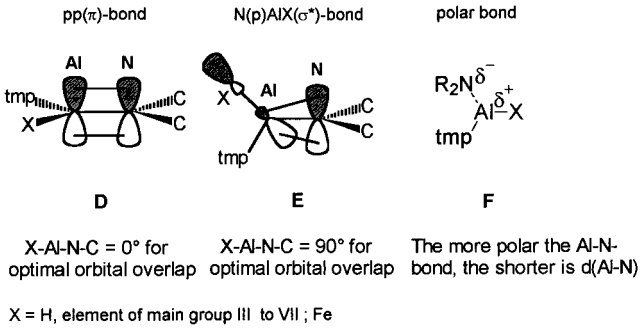

If pp(π) or N(p)AlX(σ*) interactions are responsible for the short Al−N distances, the tmp ligands should show a preference for a parallel orientation of the nitrogen lone pairs with respect to the free p_z orbital of the aluminum atom. Optimal orbital overlap for a pp(π) bond would be achieved with a C−N−Al−X torsion angle of 0°. For an N(p)AlX(σ*) bond, however, the corresponding C−N−Al−X torsion angle should be close to 90° (see Figure 19). If the Al−N bond is to be described as highly polar, these torsion angles should be a compromise between coulombic attraction ($Al^{\delta+}-N^{\delta-}$) and the steric requirements of the ligands. These three possibilities may be distinguished from a plot of d(Al−N) versus the C−N−Al−X torsion angle. Such a plot of 35 bond lengths versus the corresponding torsion angles for monomeric aminoalanes, (see Table 5) is depicted in Figure 20.

Figure 20. Plot of 35 Al−N bond lengths against the C−N−Al−X torsion angles

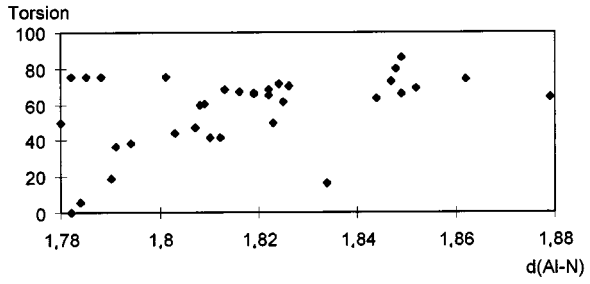

The C−N−Al−X torsion angles of short Al−N bonds reveal *no* preferential orientation of the attached ligands. Values between 0 and 80° are found for short d(Al−N) (< 1.80 A) values, indicating an absence of double bond contributions. Thus, a highly polar bonding situation for the Al−N bond is clearly the best description. Taking the geometry of the bis(tmp)borinium cation (**10a**) (linear; N−B−N angle: 180°) as the limiting case of an ideal bis(tmp)aluminum cation (**10b**), (a semiempirical AM1 calculation led to an N−Al−N angle of 171° for the tmp_2Al^+ cation)[51], for the present tmp_2AlY species **1**−**6**, the N−Al−N angle can be taken as an indicator of the extent of polarity of the Al−N bond (see Figure 21). Compounds tmp_2AlY with short, highly polar Al−N bonds, associated with loosely bound ligands R of low basicity, exhibit large N−Al−N angles, and vice versa. Figure 22 gives a graphical representation of the data collected for **1**−**6**. It can be

Table 4. Al−N distances and torsion angles of tmp_2AlY compounds

Compound	Ref.	d(Al−N) [Å]	Torsion angle [°]
tmp_2AlCl (**1a**)	[15]	1.785	75.2
		1.810	41.45
tmp_2AlBr (**1b**)	[15]	1.782	75.25
		1.812	41.23
tmp_2AlI (**1c**)	[15]	1.788	75.17
		1.803	44.2
$tmp_2AlOdipp$ (**3b**)	–	1.809	60.09
		1.808	59.45
tmp_2AlSPh (**3c**)	–	1.800	
		1.807	
		1.798	
		1.813	
tmp_2AlStBu (**3d**)	–	1.820	
		1.817	
$tmp_2AlN(H)Ph$ (**4b**)	–	1.790	18.79
		1.813	68.25
		1.822	68.7
tmp_2AlPPh_2 (**4c**)	–	1.819	65.97
		1.819	66.94
$tmp_2AlAsPh_2$ (**4d**)	–	1.816	67.55
		1.822	65.46
tmp_2AlPh (**5a**)	–	1.826	70.42
$(tmp_2Al)_2Fec$ (**5e**)	–	1.824	71.83
		1.825	61.79
$tmp_2AlSi(SiMe_3)_3$ (**5f**)	–	1.844	63.38
		1.848	79.68
$tmp_2Al-Altmp_2$ (**8**)	[48]	1.849	65.88
		1.852	68.9
$tmp_2AlFe(cp)(CO)_2$ (**2**)	[16]	1.847	73.03
		1.862	74.51
$Al[N(SiMe_3)_2]_3$	[12]	1.78	50
$trip_2AlN(H)dipp$	[56]	1.784	5.5
$t Bu_2AlNMes_2$	[14]	1.823	49.5
$t Bu_2AlN(dipp)(SiPh_3)$	[14]	1.834	16.1
$t Bu_2AlN(Ad)(SiPh)_3$	[14]	1.849	86.3
$t Bu_2AlN(SiPh_3)_2$	[14]	1.879	64.3
$MesAl[N(SiMe_3)_2]_2$	[36]	1.807	47.1
$(MeAlNdipp)_3$	[13]	1.782	0
$Al(NiPr_2)_3$	[31]	1.791	36.6
		1.794	38.3
		1.801	75.5

seen that d(Al−N) depends on the basicity of the substituent Y. Stabilized, weakly basic anions (like the halides) lead to strongly polar, short Al−N bonds, and vice versa. To obtain some appraisal of the influence of the basicity of the conjugate acid YH, the pK_a values of the Brønsted acids YH are plotted against d(Al−N) (Figure 23).

Figure 21. The N−Al−N angle as an indicator for a polar Al−N bonding situation

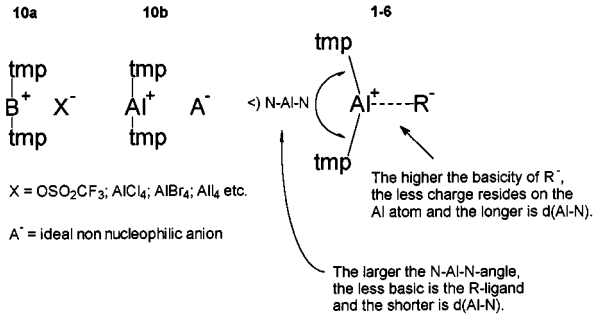

This representation reveals a good agreement with the experimental data. The insertion reaction of CO_2 with **5h** also supports the presence of a highly polar Al−N bond, as tmp_2AlMe (**5h**) possesses two reactive sites (Al−N and Al−C), of which the Al−Me site is undoubtedly also very polar. Even in the presence of excess CO_2, only the Al−N bond reacted to produce the carbaminate **5i**, leaving the Al−C bond intact. Moreover, solvolysis reactions of $tmp_2AlSi(SiMe_3)_3$ (**5f**) also support this assumption. Both the Al−N and Al−Si bonds are labile[23], but stoichiometric solvolysis reactions gave only the products of deamination, even though the Al−N bond is sterically more shielded than the Al−Si bond [cf. e.g. d(Al−N) = 1.846 Å vs. d(Al−Si) = 2.514 Å; d(C−N) = 1.50 Å vs. d(Si−Si) = 2.37 Å]. Thus, we conclude that the Al−N bonds in the present series of sterically encumbered, monomeric tmp_2AlY compounds **1**−**6** are best described as being highly polar. The degree of polarity, and thus d(Al−N), is governed by the third ligand Y.

Figure 22. Graphical representation of the dependence of d(Al−N) on the N−Al−N angles

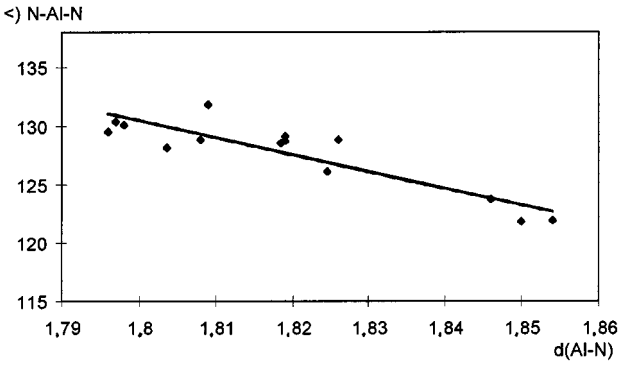

Figure 23. Plot of d(Al−N) of compounds tmp_2AlY versus the pK_a value of the corresponding Brønsted acid YH as a measure of its basicity

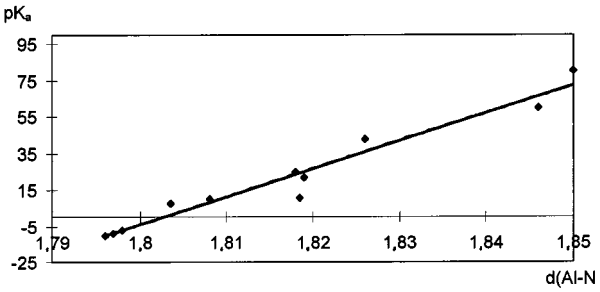

To evaluate the contributions from pp(π), N(p)AlX(σ*) and electrostatic interactions in small aminoalanes, ab initio calculations of some model compounds have been performed[17]. To understand their behavior, some results pertaining to the homologous aminoboranes are cited[10]. In the latter species, pp(π) interactions provide an additional stabilization enthalpy of up to 33 kcal/mol per B−N bond (cf. 65 kcal/mol found for the homoatomic and isoelectronic C=C double bond in ethylene)[10]. The planes around the boron and the nitrogen atoms of aminoboranes R_2NBX_2 are coplanar. In the coplanar ground state of $H_2B{=}NH_2$ (C_{2v}), d(B−N) is as short as 1.378 Å (calcd.). However, in the orthogonal transition state (C_s), the B−N distance is

elongated considerably (by about 9 pm) to 1.469 Å (calcd.). Due to saturation of the electron-deficient boron center, pp(π) contributions decrease with the attachment of an increasing number of π-donors. Applying this principle to aminoalanes, we will first discuss the results of ab initio calculations on H_2AlNH_2 (Figure 24: planar: **11a**; orthogonal: **11b**) and $Al(NH_2)_3$ (Figure 25: planar: **7d**; orthogonal: **12a**).

Figure 24. Structural parameters and results of the NBO analysis of **11a−b**

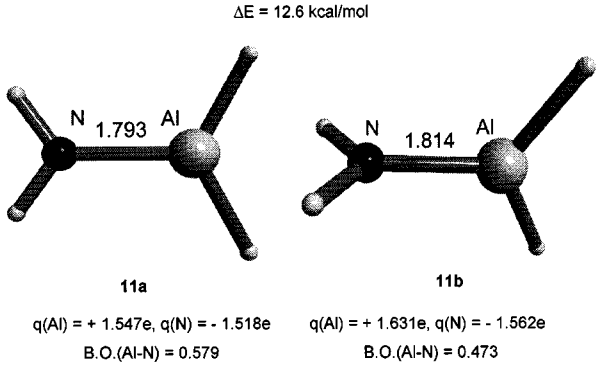

In contrast to the calculated structures for H_2BNH_2, the calculated C_{2v} structures of the planar ground state **11a** and the orthogonal transition state **11b** do not show marked differences in the values of *d*(Al−N) (1.793 vs. 1.814 Å), *d*(Al−H) (1.586 vs. 1.591 Å), Wiberg Al−N bond order (0.579 vs. 0.473) and NBO charges [*q*(Al): 1.547 vs. 1.631 e; *q*(N): −1.518 vs. −1.562 e]. Moreover, the NBO analysis reveals that in **11a** only 0.096 electrons are transferred from the N(p_z) orbital (populated with 1.905 electrons) to the 3p_z orbital of the aluminum atom. Thus, no effective pp(π) bond is formed, as is evident from the small energy difference on going to the orthogonal transition state **11b**. The pp(π) contribution amounts at most to 12.6 kcal/mol. In the transition state **11b**, which exhibits the requisite geometry for N(p)AlH(σ*) bonding, only 0.035 electrons are transferred from the N(p_z) orbital (containing 1.959 electrons) to the AlH(σ*) orbitals. Moreover, the Al−H bond is only very slightly lengthened (by 0.5 pm). These results are wholly consistent with a highly polar bonding situation, but not with effective pp(π) or N(p)AlH(σ*) bonding.

The tris(amide) $Al(NH_2)_3$ (D_{3h}) has been subjected to the same analysis in order to evaluate saturation effects, i.e. when more potential π-donors are bonded to the aluminum center (see Figure 25).

Here, the energy differences between the planar ground state **7d** and the orthogonal transition state **12a** are even smaller than those between **11a** and **11b**, even though three electronegative nitrogen atoms are present in the tris(amide), further supporting the argument for a polar bonding situation. Thus, the differences between the data for **7d** and **12a** amount to only 2.1 pm [*d*(Al−N)], 0.107 e [*q*(Al)], 0.029 e [*q*(N)] and 0.076 (Wiberg Al−N bond order). In **7d**, 0.189 electrons are transferred into the 3p_z(Al) orbital, while in **12a** only 0.043 electrons are transferred into the Al−N σ* orbital. Moreover, the pp(π) contribution per Al−N bond,

Figure 25. Structural parameters and results of the NBO analysis of **12a** and **7d**

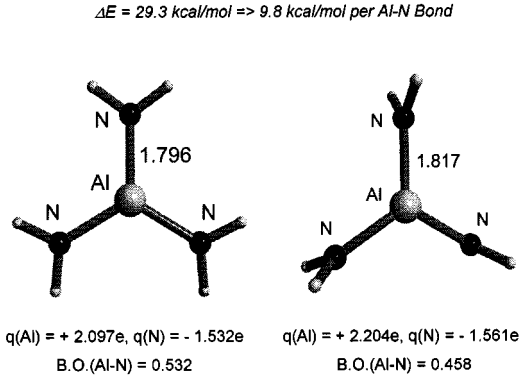

calculated by dividing the energy difference between **7d** and **12a** by three, decreases to 9.8 kcal/mol.

In the minimum energy structures of the bis(amino)alanes $(H_2N)_2AlY$ (**7a−h**) short Al−N bond lengths are associated with highly charged aluminum centers (see Table 3), and vice versa. Since only 0.15 to 0.21 electrons are transferred to the aluminum 3p_z orbitals [which negates the presence of strong pp(π) bonding] and the NBO charge on the nitrogen atoms remains essentially constant (−1.52 e to −1.54 e), the differences in the Al−N distances must be attributed to the influence of the third substituent Y. So Y has a significant effect on the charge at the aluminum atom (varying from +1.40 to +2.15 e), and, therefore, influences the coulombic interaction between Al and N, and consequently determines the Al−N bond lengths.

Conclusion

Bis(tmp)aluminum halides **1a−c** have been subjected to a series of nucleophilic substitution reactions in order to generate a systematically varied series of compounds tmp_2AlY (**2−6**). The tmp_2Al fragment not only prevents dimerization, but is also effective in stabilizing even and as yet "unusual" Al−E σ bonds (E = P, As, Si, Al, Fe). The distances *d*(Al−N) in these compounds vary from 1.782(6) to 1.862(4) Å. There is an inverse proportionality between the Al−N bond lengths and the N−Al−N bond angles. Ab initio calculations revealed the presence of very weak dative pp(π) bonding in hypothetical sterically non-demanding aminoalanes, which becomes weaker as the number of π-donors attached to the aluminum center increases. However, these pp(π) contributions (about 10 kcal/mol) are too weak to enforce on tmp_2AlY compounds geometric restrictions required to achieve optimal π-orbital overlap. Experimental and quantum mechanical results best describe the Al−N bond as being highly polar. The orientation of the tmp ligands is a compromise between the electrostatic attraction of the charged aluminum and nitrogen centers and the steric requirements of the tmp ligand. Moreover, in the tmp_2AlY system, *d*(Al−N) is a function of the pK_a value of the conjugate Brønsted acid Y−H: the stronger the acid Y−H, the higher the Al−N bond polarity and the shorter the Al−N bond lengths. Ab initio calculations reveal that

this effect can be attributed to the considerable influence that the ligand Y exerts on the charge at the aluminum atoms (variation from +1.40 to +2.15 e). Since the charge on the nitrogen atoms remains almost constant (−1.52 to −1.54 e), the differing Al−N distances can be rationalized in terms of the changing electrostatic attraction between the nitrogen and aluminum atoms, as influenced by the inductive effect of the third substitutent Y. These results not only reinforce the qualitative analysis of Al−N and Al−X bond lengths as summarized by P. J. Brothers and P. P. Power[15] but provide a much more systematic approach supported by ab initio calculations.

Investigations into the Lewis acidity of compounds tmp_2AlX (**1a−c**) and their potential to form adducts of the type tmp_2AlX*Do have been performed also. For example, the abstraction of the halide ion by strong halide abstractors with formation of ionic species $[tmp_2AlDo^+]Y^-$ (Y^- = non-nucleophilic anion) has been studied. These results will be part of forthcoming publications.

We thank the *Fonds der Chemischen Industrie* and the *Chemetall mbH* for support of our research. Moreover, we thank Mrs. *Käser* and Mrs. *Ullmann* for carrying out the C/H/N analyses, Mr. *P. Mayr*, Mr. *R. Waldhör* and Mr. *C. Miller* for recording many NMR spectra, Mrs. *D. Ewald* for mass spectra and Mrs. *E. Kiesewetter* for IR spectra.

Experimental Section

All manipulations were performed using Schlenk techniques under dinitrogen or argon. All solvents were rigorously dried prior to use and stored under N_2 or Ar. Due to insufficient protection against oxidation and hydrolysis of the air- and moisture-sensitive compounds while weighing for microanalysis, the C/H/N data are often not very accurate; Al^{3+} was determined by EDTA titration. NMR: Bruker ACP 200, Jeol GSX400 and Jeol GSX270. − IR: Nicolet FT-IR spectrometer model 6000; CsI plates, Nujol. − MS: Varian Atlas CH7 spectrometer.

tmp_2AlOPh (**3a**): Lithiation of PhOH (0.80 g, 8.5 mmol) was performed at ambient temperature in 20 ml of *n*-hexane by the addition of a solution of *n*BuLi (5.3 ml, 1.6 M, 8.5 mmol). Then, a solution of tmp_2AlBr in *n*-hexane (47.8 ml, 0.178 M, 8.5 mmol) was added at 25°C. The mixture was heated to reflux for 3−4 h. After removal of the insoluble material by filtration (0.86 g, calcd. LiBr 0.74 g), the yellowish filtrate was reduced to one-third of its original volume in vacuo and stored overnight at −20°C. 2.96 g (87%) of yellowish crystals was recovered, m.p. 80−85°C. − ^{1}H NMR (C_6D_6) (270 MHz): δ = 1.31 (t, 8 H, tmp-β-CH_2), 1.40 (s, 24 H, tmp-CH_3), 1.55 (m, 4 H, tmp-γ-CH_2), 6.8−7.4 (m, Ph-*H*, 5 H). − ^{13}C NMR (C_6D_6) (100 MHz): δ = 18.5 (tmp-γ-*C*H_2), 34.1 (tmp-*C*H_3), 39.7 (tmp-β-*C*H_2), 51.9 (N−*C*), 119.7 (Ph-*C*), 120.5 (Ph-*C*), 129.7 (Ph-*C*), 157.4 (Ph-*C*). − ^{27}Al NMR (C_6D_6) (70 MHz): δ = 75 ($\Delta_{1/2}$ = 8800 Hz). − $C_{24}H_{41}AlN_2O$ (400.59): calcd. C 71.96, H 10.00, Al 6.7, N 6.99; found C 67.99, H 10.12, Al 6.6, N 6.11.

$tmp_2AlOdipp$ (**3b**): dippOH (0.93 ml, 5.0 mmol), dissolved in 20 ml of *n*-hexane, was lithiated at ambient temperature by addition of *n*BuLi (3.2 ml, 1.6 M, 5.0 mmol) in *n*-hexane. To this solution, tmp_2AlCl in *n*-hexane (25 ml, 0.20 M, 5.0 mmol) was added and the mixture was heated for 3 h under reflux. Removal of the insoluble material by filtration yielded a yellowish solution. After reducing its volume to one-third and cooling to −78°C, yellowish crystals of **3b** (1.30 g, 54%) were formed and isolated, m.p. 97−99°C. − ^{1}H NMR (C_6D_6) (270 MHz): δ = 1.26 (t, 8 H, tmp-β-CH_2), 1.34 (s, 24 H, tmp-CH_3), 1.57 (m, 4 H, tmp-γ-CH_2), 1.27 (d, 12 H, *i*Pr-CH_3), 3.65 (sept, 2 H, Me_2C-*H*), 6.95 (dd, 1 H, Ar-*H*), 7.12 (d, Ar-*H*). − ^{13}C NMR (C_6D_6) (100 MHz): δ = 18.6 (tmp-γ-*C*H_2), 33.9, (tmp-*C*H_3), 40.2 (tmp-β-*C*H_2), 51.8 (N−*C*), 23.9 [(H)C(*C*H_3)$_2$], 26.9 [(H)*C*(CH_3)$_2$], 120.1 (Ar-*C*), 123.7 (Ar-*C*), 137.4 (Ar-*C*). − ^{27}Al NMR (C_6D_6) (70 MHz): δ = 85 ($\Delta_{1/2}$ = 9400 Hz). − $C_{30}H_{53}AlN_2O$ (484.75): calcd. C 74.33, H 11.02, Al 5.6, N 5.78; found C 71.56, H 11.27, Al 5.8, N 5.63.

tmp_2AlSPh (**3c**): Thiophenol (0.54 g, 4.9 mmol) was metallated with BuLi (4.9 mmol, 3.1 ml, 1.6 M) by stirring in hexane at −30°C. Then, tmp_2 AlBr (4.9 mmol, 25 ml of a 0.196 M solution in hexane) was added at 20°C. Stirring was continued for 14 h, and the solid material was removed by filtration. The yellow solution was then reduced in vacuo to one-third of its original volume. Cooling the solution to −78°C furnished crystals of **3c**, yield 1.0 g (49%). − ^{1}H NMR (C_6D_6) (270 MHz): δ = 1.30 (t, 8 H, tmp-β-CH_2), 1.45 (s, 24 H, tmp-CH_3), 7.00 (m, 3 H, *m*-*H*, *p*-*H*), 7.41 (m, 2 H, *o*-*H*), the tmp-γ-CH_2 protons are represented by an unresolved, very broad signal. − ^{13}C NMR (C_6D_6) (67.9 MHz): δ = 18.0 (tmp-γ-*C*H_2), 34.1 (tmp-*C*H_3), 39.2 (tmp-β-*C*H_2), 52.0 (N−*C*), 125.4 (*p*-*C*), 128.3 (*m*-*C*), 135.0 (*o*-*C*), 135.9 (1-*C*). − ^{27}Al: δ = 153 ($\Delta_{1/2}$ = 14000 Hz).

$tmp_2AlS(tBu)$ (**3d**): Prepared analogously to **3c** from *t*BuSH (0.41 g, 4.4 mmol), BuLi (2.8 ml, 1.6 M), tmp_2AlCl (4.4 mmol, 19.5 ml of a 0.228 M hexane solution). Yield 1.0 g of **3d** (58%), m.p. 87°C. − ^{1}H NMR (C_6D_6) (270 MHz): δ = 1.32 (t, 8 H, tmp-β-CH_2), 1.52 (s, 24 H, tmp-CH_3), 1.61 (s, 9 H, *t*Bu-CH_3). − ^{13}C NMR (C_6D_6) (100 MHz): δ = 18.5 (tmp-γ-*C*H_2), 34.3 (tmp-*C*H_3), 36.9 (C*Me*$_3$), 40.3 (tmp-β-*C*H_2), 44.4 (*C*Me$_3$), 52.3 (N−*C*). − ^{27}Al (C_6D_6) (70.4 MHz): δ = 152 ($\Delta_{1/2}$ = 8000 Hz). − $C_{22}H_{45}AlN_2S$ (396.65): calcd. C 66.62, H 11.43, N 7.06; found C 62.78, H 11.33, N 6.59.

$tmp_2AlNHtBu$ (**4a**): *t*BuN(H)Li (0.62 g, 7.8 mmol) was suspended in 20 ml of *n*-hexane. A solution of tmp_2AlBr (3.0 g, 7.8 mmol) in 45 ml of *n*-hexane was then added at ambient temperature. After heating the sample for 3 h under reflux, the insoluble material (0.86 g, calcd. LiBr 0.68 g) was filtered off and the filtrate reduced to one-third of its original volume and the solution stored overnight at −20°C. 1.46 g of **4a** (3.8 mmol, 49%) was recovered as a yellowish precipitate, m.p. 148−152°C. − ^{1}H NMR (C_6D_6) (400 MHz): δ = 1.45 (s, 24 H, tmp-CH_3), 1.32 (s, 9 H, *t*Bu-CH_3), 1.31 (t, 8 H, tmp-β-CH_2), 1.65 (m, 4 H, tmp-γ-CH_2). − ^{13}C NMR (C_6D_6) (100 MHz): δ = 18.7 (C2,C6), 34.3 (tmp-Me), 35.2 [C(*C*H_3)$_3$], 40.6 (C3,C5), 50.0 [*C*(CH_3)$_3$], 51.8 (C4). − ^{27}Al NMR (C_6D_6) (70 MHz): δ = 129 ($\Delta_{1/2}$ = 8900 Hz). − $C_{22}H_{46}AlN_3$ (379.61): calcd. Al 7.1; found 7.4.

$tmp_2AlNHPh$ (**4b**): Prepared as described for **4a**. PhNHLi (0.53 g, 5.3 mmol), tmp_2AlBr (48.2 ml, 0.11 M solution in *n*-hexane, 5.3 mmol). − Yield 1.32 g of **4b** (62%); m.p. 134−137°C. − ^{1}H NMR (C_6D_6) (400 MHz): δ = 1.38 (s, 24 H, tmp-CH_3), 1.31 (t, 8 H, tmp-β-CH_2), 1.65 (m, 4 H, tmp-γ-CH_2), 6.75 (t, 1 H, *p*-Ph-*H*), 7.00 (d, 2 H, *o*-Ph-*H*), 7.17 (t, 2 H, *m*-Ph-*H*). − ^{13}C NMR (C_6D_6) (100 MHz): δ = 18.8 (C2,C6), 33.9 (tmp-Me), 40.2 (C3,C5), 52.0 (C4), 117.5 (Ph-*C*), 118.7 (Ph-*C*), 129.2 (Ph-*C*), 150.3 (Ph-*C*-N). − ^{27}Al NMR (C_6D_6) (70 MHz): δ = 124 ($\Delta_{1/2}$ = 9600 Hz). − $C_{24}H_{42}AlN_3$ (399.60): calcd. Al 6.8; found 6.7.

tmp_2AlPPh_2 (**4c**): To a suspension of $LiPPh_2$ (1.19 g, 7.4 mmol) in 15 ml of *n*-hexane, a solution of tmp_2AlBr in *n*-hexane (50 ml, 0.11 M, 5.5 mmol) was added at ambient temperature and the mixture was kept for 4 h under reflux. A clear, yellow solution was removed from insoluble material by means of a syringe and reduced

in vacuo to one-third of its original volume. Storing the solution overnight at −20°C afforded 1.14 g (42%) of colorless crystals of **4c** [m.p. > 278°C (decomp.)]. − ^{1}H NMR ($CDCl_3$) (400 MHz): δ = 1.10 (t, 8 H, tmp-β-CH_2), 1.31 (s, 24 H, tmp-CH_3), 1.54 (m, 4 H, tmp-γ-CH_2), 7.10 (d, 4 H, Ar-*H*), 7.18 (t, 4 H, Ar-*H*), 7.52 (t, 2 H, Ar-*H*). − ^{13}C NMR ($CDCl_3$) (100 MHz): δ = 18.8 (tmp-γ-*C*H$_2$), 33.5 [d, ^4J(P,C) = 4.1 Hz, tmp-*C*H$_3$], 39.5 (tmp-β-*C*H$_2$), 52.0 (N-*C*), 126.2 (s, C_6H_5), 128.1 [d, ^3J(P,C) = 6.8 Hz, C_6H_5], 133.7 [d, ^2J(P,C) = 15.5 Hz, C_6H_5], 137.8 [d, ^1J(P,C) = 15.0 Hz, C_6H_5]. − ^{27}Al NMR ($CDCl_3$) (70 MHz): δ = 110 ($\Delta_{1/2}$ = 13400 Hz). − $C_{30}H_{46}AlN_2P$ (492.66): calcd. C 73.14, H 9.41, Al 5.5, N 5.69; found C 69.30, H 8.59, Al 5.5, N 4.85 (C/H/N: calcd. 15:23:1; found 16.7:24.6:1).

tmp$_2$AlAsPh$_2$ (**4d**): $LiAsPh_2$ (0.75 g, 3.2 mmol) was suspended in 20 ml of *n*-hexane and tmp$_2$AlBr (27.3 ml, 0.11 M, 3.0 mmol) in *n*-hexane was added at ambient temperature. Stirring overnight produced a yellow suspension (insoluble material as mentioned above), which was filtered off. The filtrate was reduced to one-third of its original volume and left for 4 d at −20°C. Colorless crystals of **4d** (0.93 g, 58%) separated; m.p. > 254°C (decomp.). − ^{1}H NMR ($CDCl_3$) (400 MHz): δ = 1.13 (t, 8 H, tmp-β-CH_2), 1.30 (s, 24 H, tmp-CH_3), 1.55 (m, 4 H, tmp-γ-CH_2), 7.14 (t, 4 H, Ar-*H*), 7.19 (t, 4 H, Ar-*H*), 7.54 (d, 2 H, Ar-*H*). − ^{27}Al NMR ($CDCl_3$) (70 MHz): δ = 74 ($\Delta_{1/2}$ = 18300 Hz). − $C_{30}H_{46}AlAsN_2$ (536.61): calcd. C 67.15, H 8.84, Al 5.0, N 5.22; found C 63.22, H 6.79, Al 4.9, N 5.25.

(Ph$_2$PAlI$_2$)$_3$ (**4e**): To a solution of tmp$_2$AlPPh$_2$ (0.52 g, 1.05 mmol) in 20 ml of benzene, AlI_3 (12.2 ml, 0.086 M, 1.05 mmol) in benzene was added at ambient temperature. Addition of 20 ml of *n*-pentane and cooling to 5°C led to the precipitation of 0.40 g (27%) of colorless crystals of **4e**, m.p. > 314°C (decomp.). − ^{1}H NMR (C_6D_6) (400 MHz): δ = 6.95 (m, C_6H_5, 12 H), 7.42 (t, C_6H_5, 6 H), 7.55 (t, C_6H_5, 12 H). − ^{13}C NMR (C_6D_6) (100 MHz): δ = 129.35 [d, ^3J(P,C) = 9.6 Hz], 131.35 [d, ^4J(P,C) = 11.1 Hz], 134.30 [d, ^2J(P,C) = 12.3 Hz, C_6H_5], 134.89 [d, ^1J(P,C) = 12.3 Hz, C_6H_5], 135.01 [d, ^1J(P,C) = 12.2 Hz, C_6H_5]. − ^{31}P NMR (C_6D_6) (81 MHz): δ = −42.9. − $C_{36}H_{30}Al_3I_6P_3$ (1397.89): calcd. Al 5.8, I 54.5; found Al 6.0, I 54.1.

tmp$_2$AlPh (**5a**): To a solution of tmp$_2$AlBr in *n*-hexane (50 ml, 0.11 M, 5.5 mmol), PhLi (2.42 ml, 2.27 M, 5.5 mmol) in *n*Bu$_2$O was added at ambient temperature, resulting in the immediate formation of a colorless precipitate. After stirring for 1/2 h, the suspension was allowed to settle. The clear, yellow supernatant solution was removed by means of a syringe reduced to one-third of its original volume and stored overnight at 8°C, resulting in the deposition of 1.54 g (73%) of colorless crystals of **5a**; m.p. 85−88°C. − ^{1}H NMR ($CDCl_3$) (400 MHz): δ = 1.32 (t, 8 H, tmp-β-CH_2), 1.29 (s, 24 H, tmp-CH_3), 1.66 (m, 4 H, tmp-γ-CH_2), 7.20 (d, 2 H, Ar-*H*), 7.23 (m, 1 H, Ar-*H*), 7.72 (dd, 2 H, Ar-*H*). − ^{13}C NMR ($CDCl_3$) (100 MHz): δ = 18.5 (tmp-γ-*C*H$_2$), 34.0 (tmp-*C*H$_3$), 40.6 (tmp-β-*C*H$_2$), 51.8 (N-*C*), 127.2 (s, C_6H_5), 127.8 (C_6H_5), 137.4 (C_6H_5), Al−C signal not observed. − ^{27}Al NMR ($CDCl_3$) (70 MHz): δ = 153 ($\Delta_{1/2}$ = 12300 Hz). − $C_{23}H_{41}AlN_2$ (384.43): calcd. C 74.98, H 10.75, Al 7.0, N 7.29; found C 73.19, H 9.88, Al 7.3, N 6.39.

tmp$_2$Al(nBu) (**5b**): To a solution of tmp$_2$AlBr (5.73 g, 14.8 mmol) in 80 ml of *n*-hexane, *n*BuLi (9.25 ml, 1.6 M, 14.8 mmol) in *n*-hexane was added dropwise at ambient temperature. To complete the reaction, the mixture was stirred for 1 h at ambient temperature. After removal of the insoluble material, the solvent of the yellow filtrate was removed in vacuo providing **5b** as a viscous oil, which could not be crystallized from various solvents. Yield 5.23 g (97%). − ^{1}H NMR ($CDCl_3$) (270 MHz): δ = 1.31 (t, 8 H, tmp-β-CH_2), 1.36 [s, 24 H, tmp-C(CH_3)$_2$], 1.65 (m, 4 H, tmp-γ-CH_2), 0.39 (t, 2 H, Bu-α-CH_2), 1.10 (t, 3 H, Bu-CH_3), 1.23 and 1.47 (2 m, each 2 H, β- and γ-CH_2). − ^{13}C NMR (C_6D_6) (100 MHz): δ = 18.7 (tmp-*C*4), 34.1 (tmp-*C*7−10), 40.5 (tmp-*C*3/5), 51.9 (tmp-*C*2/6), 14.1 (Bu-*C*4), 28.4 (Bu-*C*3), 29.1 (Bu-*C*2), Al−C signal not observed. − ^{27}Al NMR ($CDCl_3$) (70 MHz): δ = 164 ($\Delta_{1/2}$ = 13400 Hz). − MS: *m*/*z* = 364 [tmp$_2$AlnBu$^+$].

tmp$_2$AlC$_6$H$_4$OCH$_3$ (**5c**): A solution of *p*-bromoanisole (0.63 ml, 5.0 mmol) in 20 ml of THF was refluxed for 1 h with 0.13 g of Mg and then cooled to ambient temperature. To this Grignard solution (assuming 100% conversion), tmp$_2$AlBr (18.7 ml, 0.268 M, 5.0 mmol) in *n*-hexane was added and the mixture was refluxed overnight. After filtration, the collected precipitate (1.67 g) was extracted with 20 ml of CH_2Cl_2 (the insoluble material subsequently weighed 0.93 g). The combined filtrates were reduced to one-third of the original volume and then stored overnight at −20°C to yield 1.61 g (79%) of **5c** as a microcrystalline precipitate, m.p. > 100°C (decomp.). − ^{1}H NMR ($CDCl_3$) (400 MHz): δ = 1.36 (t, 8 H, tmp-β-CH_2), 1.34 [s, 24 H, tmp-C(CH_3)$_2$], 1.70 (m, 4 H, tmp-γ-CH_2), 3.79 (s, 3 H, O-CH_3), 6.85 (d, 2 H, Ar-*H*), 7.70 (d, 2 H, Ar-*H*). − ^{13}C NMR ($CDCl_3$) (100 MHz): δ = 18.6 (tmp-*C*4), 33.8 (tmp-*C*7−10), 40.6 (tmp-*C*3/5), 51.6 (tmp-*C*2/6), 54.6 (O-*C*H$_3$), 113.0, 139.1, 159.9 (Ar-*C*), Al−C signal not observed. − ^{27}Al NMR ($CDCl_3$) (70 MHz): δ = 160 ($\Delta_{1/2}$ = 19400 Hz). − $C_{25}H_{43}AlN_2O$ (414.61): calcd. Al 6.5; found Al 6.7.

(tmp$_2$Al)$_2$C$_2$B$_{10}$H$_{10}$ (**5d**): To a solution of 1,2-dicarba-*closo*-dodecaborane(12) (1.0 g, 6.9 mmol) in 20 ml of toluene, *n*BuLi in *n*-hexane (40.6 ml, 1.6 M, 64.9 mmol) (cooled to 0°C) was added dropwise over a period of 20 min. After 5 min, a colorless precipitate of 1,2-dilithio-1,2-dicarba-*closo*-dodecaborane started to separate. The mixture was then stirred for a further 1.5 h to ensure completion of the reaction. The precipitate was isolated by filtration, washed with two 20-ml portions of *n*-pentane, and dried in vacuo. The resulting colorless, pyrophoric powder was suspended in 40 ml of *n*-pentane and treated at −78°C with a solution of tmp$_2$AlI (6.1 g, 14 mmol, in 50 ml of *n*-hexane). The mixture was allowed to warm to room temperature, and stirring was continued for 2 d. Removal of the insoluble material by filtration left a yellow solution, from which the solvent was removed in vacuo. The nonvolatile, yellow-brownish oil was rigorously dried in vacuo and then subjected to analysis. Yield 2.57 g of **5d** (3.4 mmol, 49%). − ^{1}H NMR ($CDCl_3$) (270 MHz): δ = 1.29 (t, 8 H, tmp-β-CH_2), 1.32 [s, 24 H, tmp-C(CH_3)$_2$], 1.64 (m, 4 H, γ-CH_2). − ^{13}C NMR ($CDCl_3$) (100 MHz): δ = 18.3 (tmp-*C*4), 33.9 (tmp-*C*7−10), 40.2 (tmp-*C*3/5), 51.7 (tmp-*C*2/6), Al−C signal not observed. − ^{27}Al NMR ($CDCl_3$) (70 MHz): δ = 164 ($\Delta_{1/2}$ = 12300 Hz). − ^{11}B NMR ($CDCl_3$) (86.4 MHz): δ = −15.0 [(^1J(B,H) = 173.3 Hz], −13.8 [^1J(B,H) = 169.2 Hz], −11.7 [^1J(B,H) not resolved], −9.4 [^1J(B,H) = 161.8 Hz], −7.1 [^1J(B,H) = 187.3 Hz], −2.6 [^1J(B,H) = 145.0 Hz]. − $C_{38}H_{82}Al_2B_{10}N_4$ (757.16): calcd. C 60.28, H 10.92, N 7.40; found C 59.35, H 10.87, N 7.64.

(tmp$_2$Al)$_2$Fec (**5e**): $FecLi_2$ (1.1 g, 5.5 mmol) was suspended in 20 ml of *n*-hexane and tmp$_2$AlCl in *n*-hexane (50 ml, 0.20 M, 5.0 mmol) was added at ambient temperature. After stirring overnight, the insoluble material was removed by filtration and the resulting red filtrate was reduced to one-third of its original volume. Storage of the solution overnight at −20°C led to the deposition of red crystals of **5e** (2.10 g, 48%), m.p. 176−179°C. − ^{1}H NMR (C_6D_6) (400 MHz): δ = 1.45 (t, 8 H, tmp-β-CH_2), 1.57 (s, 24 H, tmp-CH_3), 1.73 (m, 4 H, tmp-γ-CH_2), 4.47 (t, 4 H, cp-*H*), 4.55 (t, 4 H, cp-*H*). − ^{13}C NMR (C_6D_6) (100 MHz): δ = 18.6 (tmp-γ-*C*H$_2$), 34.3 (tmp-*C*H$_3$), 40.6 (tmp-β-*C*H$_2$), 52.0 (N-*C*), 71.9 (C_5H_4Al), 79.1

Table 5. Crystallographic data and relevant data referring to the structure solution and refinement

Compound	$tmp_2AlOdipp$ (**3b**)	tmp_2AlSPh (**3c**)	$tmp_2AlStBu$ (**3d**)	$tmp_2AlN(H)Ph$ (**4b**)tmp_2AlPPh_2 (**4c**)	$tmp_2AlAsPh_2$ (**4d**)	$(I_2AlPPh_2)_3$ (**4e**)
Code	Kros31	Knab7	Knabe8	Kros16	Ingo10	Ingo13	Kros22
Chem. formula	$C_{30}H_{53}AlN_2O$	$C_{24}H_{41}AlN_2S$	$C_{22}H_{45}AlN_2S$	$C_{36}H_{72}Al_2N_4$	$C_{30}H_{46}AlN_2P$	$C_{30}H_{46}AlAsN_2$	$C_{15}H_{13}AlI_2P$
Formula weight	484.72	416.63	396.64	614.94	492.64	536.59	505.02
Cryst. size [mm]	0.2 × 0.2 × 0.3	0.4 × 0.5 × 0.5	0.2 × 0.3 × 0.4	0.2 × 0.32 × 0.6	0.3 × 0.3 × 0.4	0.5 × 0.5 × 0.6	0.12 × 0.2 × 0.4
Cryst. system	monoclinic	monoclinic	monoclinic	monoclinic	triclinic	triclinic	trigonal
Space group	$P2_1/c$	$P2(1)/n$	$P2(1)/n$	$C2/c$	$P1$	$P1$	$R3$
a [A]	17.008(1)	8.3000(14)	10.5638(2)	21.264(9)	10.1560(1)	10.156(3)	23.45920(1)
b [A]	10.760(8)	41.673(8)	14.66050(10)	7.876(4)	10.5220(1)	10.652(6)	23.45920(1)
c [A]	17.449(1)	14.044(2)	15.5048(2)	24.426(9)	15.154(7)	15.239(9)	23.45920(1)
α [°]	90	90.00	90.00	90	98.98(2)	98.93(5)	106.47
β [°]	110.462(1)	96.120(7)	96.84(1)	114.058(8)	90.51(2)	90.80(4)	106.47
γ [°]	90	90.00	90.00	90	117.980(1)	118.10(4)	106.47
V [A^3]	2991.8(4)	4829.9(14)	2384.15(6)	3735.5(3)	1406.3(7)	1429.4(1)	10902.49(8)
Z	4	8	4	4	2	2	24
$\rho_{calcd.}$ [Mg/m^3]	1.076	1.146	1.105	1.093	1.163	1.247	1.846
μ [mm^{-1}]	0.091	0.182	0.181	0.094	0.150	1.240	3.584
F(000)	1072	1824	880	1368	536	572	5688
Index range	$-21 \le h \le 21$	$-10 \le h \le 10$	$-13 \le h \le 13$	$-26 \le h \le 24$	$-3 \le h \le 11$	$0 \le h \le 11$	$-26 \le h \le 24$
Index range	$-13 \le k \le 13$	$-51 \le k \le 47$	$-18 \le k \le 16$	$-10 \le k \le 10$	$-11 \le k \le 10$	$-12 \le k \le 10$	$-25 \le k \le 25$
Index range	$-21 \le l \le 21$	$-16 \le l \le 15$	$-19 \le l \le 20$	$-33 \le l \le 25$	$-17 \le l \le 17$	$-18 \le l \le 18$	$-25 \le l \le 25$
2θ [°]	54.72	55.44	58.26	58.16	47.98	50.10	46.50
T [K]	193	183	193	213	223	233	193
Refl. collected	13267	21001	13292	9285	4611	4688	46312
Refl. unique	5691	7098	4779	3772	4335	4386	10154
Refl. observed (4σ)	3170	6131	2626	2794	3249	3633	7757
R_{int}	0.0474	0.0553	0.0513	0.0881	0.0213	0.0259	0.0890
No. of variables	319	521	246	199	315	315	685
Weighting scheme[a] x/y	0.0075/2.6126	0.0250/4.9687	0.0187/2.1682	0.0560/6.0270	0.0383/0.5694	0.0510/1.2191	0.0254/44.7300
GooF	1.163	1.214	1.186	1.193	1.030	1.038	1.186
Final R (4σ)	0.0543	0.0508	0.0476	0.0668	0.0405	0.0399	0.0427
Final $wR2$	0.0995	0.1151	0.0919	0.1473	0.0879	0.0934	0.0791
Larg. res. peak [e/A^3]	0.301	0.488	0.216	0.325	0.220	0.521	0.989

[a] $w^{-1} = \sigma^2 F_o^2 + (xP)^2 + yP$; $P = (F_o^2 + 2F_c^2)/3$.

(C_5H_4Al), Al−C signal not observed. − ^{27}Al NMR (C_6D_6) (70 MHz): δ = 59 ($\Delta_{1/2}$ = 7400 Hz). − $C_{46}H_{80}Al_2FeN_4$ (798.98): calcd. C 69.15, H 10.09, Al 6.8, N 7.01; found C 63.59, H 9.04, Al 6.5, N 6.27 (C/H/N: calcd. 11.50:20:1; found 11.77:19.93:1).

$tmp_2AlSi(SiMe_3)_3$ (**5f**): To a stirred solution of $(Me_3Si)_3SiLi{\cdot}3$ thf[52] (1.01 g, 2.14 mmol) in 30 ml of *n*-hexane, was added a solution of tmp_2AlBr (0.83 g, 2.14 mmol) in 12 ml of *n*-hexane. After stirring overnight, the solvent was evaporated in vacuo. The residue was extracted with 20 ml of *n*-pentane, filtered, and the filtrate reduced to one-third of its original volume. Cooling of the yellow solution overnight at −20°C led to the deposition of 0.76 g (65%) of colorless crystals of **5f**, m.p. 203−206°C. (^{1}H-NMR and ^{13}C-NMR spectra at various temperatures are depicted in the text). − ^{1}H NMR (C_6D_6) (270 MHz): δ = 0.44 [s, 27 H, $Si(CH_3)_3$], 1.36 (t, 8 H, tmp-β-CH_2), 1.49 [s, 24 H, tmp-$C(CH_3)_2$], 1.63 (m, 4 H, tmp-γ-CH_2). − ^{13}C NMR (C_6D_6) (100 MHz): δ = 5.3 [$Si(CH_3)_3$], 18.6 (tmp-*C*4), 33.8 (tmp-*C*7−10), 41.4 (tmp-*C*3/5), 53.1 (tmp-*C*2/6). − ^{27}Al NMR (C_6D_6) (70 MHz): δ = 186 ($\Delta_{1/2}$ = 12400 Hz). − ^{29}Si NMR (C_6D_6) (55 MHz): δ = −7.9. − $C_{27}H_{63}AlN_2Si_4$ (555.13): calcd. C 58.42, H 11.44, Al 4.9, N 5.05; found C 55.99, H 11.52, Al 5.0, N 4.92 (C/H/N: calcd. 13.50:31.50:1; found 13.27:32.54:1).

tmp_2AlMe (**5h**) *and $[(tmpCO_2)_2AlMe]_2$* (**5i**): To a solution of tmp_2AlCl (40 ml, 0.20 M, 8.0 mmol) in *n*-hexane, 10 ml of a freshly prepared solution of $LiSnMe_3$ (1.0 M, 10.0 mmol) in THF was added over a period of 30 min. After stirring the mixture overnight, all volatile materials were removed in vacuo and the residue was extracted with 30 ml of *n*-pentane. From a portion of this solution all volatiles were removed in vacuo and the maining oil was subjected to analysis by NMR and mass spectrometry and proved to be **5h**. − ^{1}H NMR (C_6D_6) (60 MHz): δ = −0.24 (s, 3 H, Al-CH_3), 1.45 (s, 24 H, tmp-CH_3), 1.40 (t, 8 H, tmp-β-CH_2), 1.70 (m, 4 H, tmp-γ-CH_2). − ^{13}C NMR (C_6D_6) (100 MHz): δ = −1.0 [Al(*C*H_3)], 18.5 (tmp-*C*4), 34.3 (tmp-*C*7−10), 40.4 (tmp-*C*3/5), 52.0 (tmp-*C*2/6). − ^{27}Al NMR (C_6D_6) (70 MHz): δ = 173. − MS (70 eV, 30°C): *m*/*z* (%) = 322 (41) [$tmp_2AlMe^{+\cdot}$].

Since crystals of **5h** could not be obtained from the *n*-pentane solution, 5 ml of diethyl ether was added. The solution was then cooled to −78°C (dry-ice). During the course of several weeks, CO_2 slowly diffused into the vessel and underwent insertion into the Al−N bonds, resulting in the deposition of colorless crystals of **5i** (1.93 g, 29%), m.p. 140−142°C. − ^{1}H NMR (C_6D_6) (400 MHz): (monomer): δ = −0.24 (br. s, Al-CH_3), 1.30 (t, 8 H, tmp-β-CH_2), 1.56 (s, 24 H, tmp-CH_3); (dimer): δ = −0.24 (br. s, Al-CH_3), 1.41, 1.44 (2 t, each 8 H, tmp-β-CH_2), 1.61, 1.64 (2 s, each 24 H, tmp-CH_3). − ^{13}C NMR (C_6D_6) (100 MHz): (monomer): δ = 16.2 (tmp-γ-*C*H_2), 29.3 (tmp-*C*H_3), 42.0 (tmp-β-*C*H_2), 57.3 (N-*C*), 170.1 (N-*C*O_2), Al−C signal not observed; (dimer): δ = 15.3, 16.5 (tmp-γ-*C*H_2), 29.7, 29.9 (tmp-*C*H_3), 39.4, 42.7 (tmp-β-*C*H_2), 57.0, 57.2 (N−*C*), 160.9 (N−*C*O_2), Al−C signal not observed. − ^{27}Al NMR (C_6D_6) (70 MHz): (monomer): δ = 21 ($\Delta_{1/2}$ = 1120 Hz); (dimer): δ = 9 ($\Delta_{1/2}$ = 980 Hz). − IR (Nujol): ν = 1582 cm^{-1}, ν(C=N)].

Table 5 *(Continued)*

Compound	tmp_2AlPh (**5a**)	$(tmp_2Al)_2Fec$ (**5e**)	Carbaminate (**5i**)	$tmp_2AlSi(SiMe_3)_3$ (**5f**)
Code	Kros21	Kros32	Kros33	Kros11
Chem. formula	$C_{24}H_{41}AlN_2$	$C_{46}H_{80}Al_2FeN_4$	$C_{45.33}H_{86}Al_2N_4O_8$	$C_{27}H_{63}AlN_2Si_4$
Formula weight	384.57	798.95	869.16	555.13
Cryst. size [mm]	0.5 × 0.5 × 0.7	0.15 × 0.2 × 0.3	0.1 × 0.2 × 0.2	0.25 × 0.25 × 0.45
Cryst. system	monoclinic	orthorhombic	monoclinic	triclinic
Space group	*C*2/*c*	*Pbcn*	*P*2(1)/*c*	*P*1
a [A]	11.256(6)	25.07(2)	11.61950(10)	11.418(1)
b [A]	20.869(1)	18.67(1)	11.299	11.915(1)
c [A]	10.672(5)	9.805(6)	20.827	16.129(2)
α [°]	90	90	90.00	93.17(1)
β [°]	113.11(1)	90	93.5030(10	109.08(1)
γ [°]	90	90	90.00	118.48(1)
V [A^3]	2305.7(2)	4589(5)	2729.11(2)	1762.9(3)
Z	4	4	2	2
$\rho_{calcd.}$ [Mg/m^3]	1.108	1.156	1.058	1.046
μ [mm^{-1}]	0.099	0.401	0.101	0.211
F(000)	848	1744	952	616
Index range	$-14 \le h \le 14$	$-32 \le h \le 32$	$-14 \le h \le 14$	$-11 \le h \le 9$
Index range	$-25 \le k \le 25$	$-23 \le k \le 24$	$-14 \le k \le 14$	$-13 \le k \le 12$
Index range	$-13 \le l \le 13$	$-11 \le l \le 12$	$-22 \le l \le 26$	$-18 \le l \le 18$
2θ [°]	57.50	55.10	58.40	49.00
Temp, [K]	193(3)	193	173	198
Refl. collected	6410	18335	15176	8085
Refl. unique	1956	4756	5308	5661
Refl. observed (4σ)	1235	3097	3231	4600
R_{int}	0.0565	0.0473	0.1065	0.0466
No. of variables	128	248	282	324
Weighting scheme[a] x/y	0.0564/3.2577	0.0249/5.6830	0.0980/4.2353	0.0411/0.7067
GooF	1.165	1.190	1.122	1.051
Final *R* (4σ)	0.0557	0.0537	0.0793	0.0393
Final *wR*2 °	0.1278	0.1062	0.2070	0.0950
Larg. res. peak [e/A^3]	0.227	0.356	0.901	0.308

− $C_{42}H_{78}Al_2N_4O_8$ (821.07): calcd. C 61.44, H 9.58, Al 5.1, N 6.82; found C 60.60, H 9.36, Al 5.0, N 6.72.

[(Me$_3$Si)$_3$Si(OEt)Al(μ-OEt)]$_2$ (**5j**): To a stirred solution of $tmp_2AlSi(SiMe_3)_3$ (0.78 g, 1.8 mmol) in 25 ml of *n*-hexane, was added 10 ml (3.5 mmol) of a 2% EtOH solution in *n*-hexane. The turbid mixture was exposed to ultrasound for 24 h and then filtered. The yellow filtrate thus obtained was reduced in vacuo to a volume of 5 ml and stored at −20°C, resulting in the deposition of 0.56 g (85%) of colorless crystals of **5j**. − ^{1}H NMR (C_6D_6) (270 MHz): δ = 0.17 [s, 54 H, Si(C*H*$_3$)$_3$], 1.20 (t, 6 H, OCH$_2$C*H*$_3$), 1.28 (t, 6 H, μ-OCH$_2$C*H*$_3$), 4.13 (q, 4 H, μ-OC*H*$_2$), 3.86 (q, 4 H, OC*H*$_2$). − ^{27}Al NMR (C_6D_6) (70 MHz): δ = 42.2 ($\Delta_{1/2}$ = 1660 Hz). − $C_{26}H_{74}Al_2O_4Si_8$ (729.53): calcd. Al 7.4; found 7.1.

[(PhO)$_3$AlSi(SiMe$_3$)$_3$]tmpH$_2$ (**5k**): To a stirred solution of $tmp_2AlSi(SiMe_3)_3$ (0.87 g, 2.0 mmol) in 25 ml of diethyl ether and 25 ml of *n*-hexane powdered phenol (0.37 g, 4.0 mmol) was added. The resulting suspension was stirred overnight, insoluble material filtered off, and the filtrate reduced in vacuo to a volume of 20 ml. Crystals of **5k** separated: yield 1.05 g (76%), m.p. 145−147°C. − ^{1}H NMR ($CDCl_3$) (400 MHz): δ = −0.04 [s, 27 H, Si(C*H*$_3$)$_3$], 1.36 (s, 12 H, tmp-C*H*$_3$), 1.45 [t, 4 H, ^{3}*J*(H,H) = 5.5 Hz, tmp-β-C*H*$_2$], 1.57 (m, 2 H, tmp-γ-C*H*$_2$), 6.78 [t, 3 H, ^{3}*J*(H,H) = 7.4 Hz, OPh-δ-C*H*], 6.97 [d, 6 H, ^{3}*J*(H,H) = 7.1 Hz, OPh-γ-C*H*], 7.17 [t, 6 H, ^{3}*J*(H,H) = 7.7 Hz, OPh-β-C*H*]. − ^{13}C NMR ($CDCl_3$) (100 MHz): δ = 3.4 [Si(*C*H$_3$)$_3$], 16.2 (tmp-*C*4), 28.3 (tmp-*C*H$_3$), 36.2 (tmp-*C*3/5), 57.4 (tmp-*C*2/6), 118.4 (OPh-β-*C*H), 120.5 (OPh-γ-*C*H), 129.5 (OPh-δ-*C*H), 158.7 (OPh-α-*C*H). − ^{27}Al NMR ($CDCl_3$) (70 MHz): δ = 91 ($\Delta_{1/2}$ = 1000 Hz). − ^{29}Si NMR ($CDCl_3$) (55 MHz): δ = −8.7. − IR (Nujol): ν = 3076 cm^{-1} [ν(N−H)]. − $C_{36}H_{62}AlNO_3Si_4$ (694.20): calcd. C 62.11, H 8.98, N 2.01; found C 60.57, H 8.80, N 2.1 (C/H: calcd. 1:1.72; found 1:1.73).

[(Me$_3$Si)$_3$SiAlCl$_3$][tmpH$_2$] (**5l**): To a stirred solution of $tmp_2AlSi(SiMe_3)_3$ (0.55 g, 1.25 mmol) in 40 ml of *n*-hexane at −70°C, was added HCl (21.9 ml of a 0.225 M solution of HCl in diethyl ether, 5.0 mmol). The mixture was then allowed to warm to ambient temperature and stirring was continued overnight. The insoluble material was filtered off, all volatiles from the solution were removed in vacuo, and the residue was dissolved in 15 ml of CH_2Cl_2. Cooling of this solution overnight at −20°C afforded colorless crystals of **5l**. Yield 0.41 g (65%), m.p. 154−155°C. − ^{1}H NMR ($CDCl_3$) (400 MHz): δ = 0.16 [s, 27 H, Si(C*H*$_3$)$_3$], 1.25 (m, 4 H, tmp-γ-C*H*$_2$), 1.52 (s, 24 H, tmp-C*H*$_3$), 1.67 (m, 8 H, tmp-β-C*H*$_2$). − ^{13}C NMR ($CDCl_3$) (100 MHz): δ = 0.9 [Si(*C*H$_3$)$_3$], 22.9 (tmp-*C*4), 35.0 (tmp-*C*7−10), 38.6 (tmp-*C*3/5), 58.0 (tmp-*C*2/6). − ^{27}Al NMR ($CDCl_3$) (70 MHz): δ = 133 ($\Delta_{1/2}$ = 3000 Hz). − ^{29}Si NMR ($CDCl_3$) (55 MHz): δ = −8.5. − $C_{18}H_{47}AlCl_3NSi_4$ (523.26): calcd. C 46.27, H 9.63, N 4.00; found C 45.79, H 9.50, N 3.64. − Crystal structure analysis was carried out with a crystal of the composition $[(Me_3Si)_3SiAlCl_3][tmpH_2][tmpH_2]Cl \cdot 0.25\ OEt_2$.

tmp$_2$AlH$_2$BH$_2$ (**6a**): A suspension of $LiBH_4$ (0.070 g, 3.3 mmol) in 20 ml of *n*-hexane was cooled to −78° C, and a solution of tmp_2AlBr (0.64 g, 1.7 mmol) in 5 ml of *n*-hexane was added dropwise. The mixture was then allowed to warm to ambient temperature and stirred overnight. Removal of the insoluble material by filtration yielded a yellow solution, which was reduced to a volume of 15 ml and stored overnight at −20°C. The resulting precipitate of **6a** (0.23 g, 42%) melted with decomposition at $T > 316$°C. − ^{1}H NMR (C_6D_6) (270 MHz): δ = 1.37 (s, 24 H, tmp-C*H*$_3$), 1.25 (t, 8 H, tmp-β-C*H*$_2$), 1.57 (m, 4 H, tmp-γ-C*H*$_2$). − ^{13}C NMR (C_6D_6) (100 MHz): δ = 52.5 (tmp-*C*2,6), 40.5 (tmp-β-*C*H$_2$), 34.0 (tmp-*C*H$_3$), 18.5 (tmp-γ-*C*H$_2$). − ^{11}B NMR (C_6D_6) (64 MHz): δ = −24.4 (quint) [^{1}*J*(B−H) = 85 Hz]. − ^{27}Al NMR (C_6D_6) (70 MHz):

Table 5 *(Continued)*

Compound	$Cl_3AlSi(SiMe_3)_3^-$ (**5l**)	$(Me_3Si)_3SiAl(OPh)_3^-$ (**5k**)	$[(Me_3Si)_3SiAlOEt_2]_2$ (**5j**)	tmp_2AlH_2(9-BBN) (**6b**)
Code	Kros17	Kros15	Kros19	Kros20
Chem. formula	$C_{28}H_{69.50}AlCl_4N_2Si_4O_{0.25}$	$C_{36}H_{62}AlNO_3Si_4$	$C_{13}H_{37}AlO_2Si_4$	$C_{26}H_{52}AlBN_2$
Formula weight	715.50	696.21	364.77	430.49
Cryst. size [mm]	0.2 × 0.1 × 0.1	0.3 × 9.3 × 0.2	0.24 × 0.3 × 0.6	0.2 × 0.3 × 0.4
Cryst. system	monoclinic	monoclinic	monoclinic	monoclinic
Space group	$P2_1/c$	$P2_1/n$	$P2_1/c$	$C2/c$
a [A]	17.59(2)	19.76(3)	9.2471(6)	13.2641(3)
b [A]	11.10(1)	12.05(2)	17.294(1)	19.7133(3)
c [A]	24.88(3)	20.35(3)	15.492(1)	10.9173(2)
α [°]	90	90	90	90
β [°]	108.7(3)	118.95(4)	106.891(1)	107.0650(1)
γ [°]	90	90	90	90
V [A^3]	4601(1)	4240(1)	2370.7(3)	2728.88(6)
Z	4	4	4	4
$\rho_{calcd.}$ [Mg/m^3]	1.033	1.091	1.022	1.048
μ [mm^{-1}]	0.399	0.192	0.288	0.089
F(000)	1554	1512	800	960
Index range	$-19 \le h \le 19$	$-25 \le h \le 25$	$-10 \le h \le 12$	$-25 \le k \le 25$
Index range	$-12 \le k \le 11$	$-15 \le k \le 15$	$-21 \le k \le 22$	$-25 \le k \le 25$
Index range	$-27 \le l \le 26$	$-25 \le l \le 24$	$-19 \le l \le 19$	$-13 \le l \le 11$
2θ [°]	46.5	58.22	57.44	57.08
T [K]	293(2)	293(2)	213	193
Refl. collected	17137	20920	11446	7410
Refl. unique	6411	8896	4797	2524
Refl. observed (4σ)	4878	5993	1934	1242
R_{int}	0.0500	0.0571	0.1124	0.1337
No. Variables	367	425	191	146
Weighting scheme[a] x/y	0.0765/4.8394	0.0374/3.7774	0.0330/5.2990	0.1397/8.4413
GooF	1.106	1.076	1.089	1.245
Final R (4σ)	0.0598	0.0471	0.0671	0.0802
Final $wR2$	0.1535	0.1026	0.1280	0.2517
Larg. res. peak [e/A^3]	0.315	0.636	0.346	0.299

[a] $w^{-1} = \sigma^2F_o^2 + (xP)^2 + yP$; $P = (F_o^2 + 2F_c^2)/3$.

δ = 125 ($\Delta_{1/2}$ = 7040 Hz). − IR (Nujol): $\tilde{\nu}$ [ν(B−H) region] = 2289 cm^{-1} vs, 2317 vs, 2341 vs, 2403 vs, 2455 m. − MS: m/z = 322 [$tmp_2AlH_2BH_2^+$]. − $C_{18}H_{40}AlBN_2$ (322.32): calcd. Al 8.4; found Al 8.9.

tmp_2AlH_2(9-BBN) (**6b**): LiH_2(9-BBN) (1.52 g, 6.25 mmol) was suspended in 20 ml of *n*-hexane. At ambient temperature, 25 ml of a 0.20 M *n*-hexane solution of tmp_2AlCl (5.0 mmol) was added and the mixture was stirred overnight. The clear, yellow solution was then reduced to one-third of its original volume. Cooling of the solution overnight at −20°C afforded 1.59 g (74%) of colorless crystals of **6b**, m.p. > 288°C (decomp.). − ^1H NMR (C_6D_6) (400 MHz): δ = 1.39 (s, 24 H, tmp-CH_3), 1.23 (t, 8 H, tmp-β-CH_2), 1.58 (m, 4 H, tmp-γ-CH_2), 1.60−2.20 (m, 14 H, 9-BBN-CH_2). − ^{13}C NMR (C_6D_6) (100 MHz): δ = 52.2 (tmp-*C*2,6), 41.1 (tmp-β-*C*H_2), 33.6 (tmp-*C*H_3), 18.4 (tmp-γ-*C*H_2), 24.6 (9-BBN-*C*H_2), 34.6 (9-BBN-*C*H_2), B−C signal not observed. − ^{11}B NMR (C_6D_6) (64 MHz): δ = −3.0 (s, $\Delta_{1/2}$ = 207.4 Hz ^1H-decoupled; $\Delta_{1/2}$ = 246.7 Hz ^1H-coupled). − ^{27}Al NMR (C_6D_6) (70 MHz): δ = 115 ($\Delta_{1/2}$ = 10700 Hz). − IR (Nujol): ν [ν(B−H) region] = 1706 cm^{-1} w, 1753 w, 1788 w, 1824 m, 1859 m, 1895 s, 1911 vs, 1955 vs, 1997 vs, 2057 s, 2200 w. − $C_{26}H_{52}AlBN_2$ (430.51): calcd. C 72.54, H 12.18, Al 6.3, N 6.51; found C 67.86, H 11.55, Al 6.4, N 5.54 (C/H/N: calcd. 13:26:1; found 14.28:28.97:1; C/H: calcd. 1:2; found 1:2.02).

X-ray Crystal Structure Determinations: Data collection for X-ray structure determinations was performed with a Syntex P4 or a Syntex R3 four-circle diffractometer, using graphite-monochromated Mo-K_α (0.71073 A) radiation. Single crystals were mounted in Lindemann capillaries and sealed under argon. Other data collections for X-ray structure determinations were performed with a Syntex P4 four-circle diffractometer equipped with a CCD area detector[53]. Single crystals were mounted in polyfluoroether oil and fixed on top of a glass fibre. Data collections were carried out at −80 to −100°C. All calculations were performed on PCs and workstations using the Siemens SHELXTL-Plus[54] or SHELX-93[55] software packages. The structures were solved by direct or heavy-atom methods and successive interpretation of the difference Fourier maps, followed by least-squares refinement. All non-hydrogen atoms were refined anisotropically. Hydrogen atoms were included in the final refinement in calculated positions by a riding model using fixed isotropic parameters. Relevant data relating to the crystallography, data collection and refinement are compiled in Table 4. Further details on the crystal structure determinations have been deposited with the Cambridge Crystallographic Data Centre and may requested by quoting the depository number CCDC-101483, the names of the authors, and the full journal citation.

[1] I. Krossing, Dissertation, University of Munich, **1997**.
[2] X-ray structure determinations.
[3] R. West, *Angew. Chem.* **1987**, *99*, 1231−1245; *Angew. Chem. Int. Ed. Engl.* **1987**, *26*, 1201.
[4] S. Masamune, *Angew. Chem.* **1991**, *103*, 916−937; *Angew. Chem. Int. Ed. Engl.* **1991**, *30*, 902.
[5] L. F. Guselnikov, N. S. Nametkin, *Chem. Rev.* **1979**, *79*, 529−577.
[6] H. Nöth, *Angew. Chem.* **1988**, *100,* 1664−1684; *Angew. Chem. Int. Ed. Engl.* **1988**, *27*, 1603.
[7] [7a] R. T. Paine, H. Nöth, *Chem. Rev.* **1995**, *95*, 343−379. − [7b] G. Linti, H. Nöth, R.T. Paine, *Chem. Ber.* **1993**, *126*, 875−887.
[8] H. G. von Schnering, M. Somer, M. Hartweg, K. Peters, *Angew. Chem.* **1990**, *102*, 6364; *Angew. Chem. Int. Ed. Engl.* **1990**, *29*, 5758.
[9] M. F. Lappert, P. P. Power, A. R. Sanger, R. C. Srivastava, *Me-*

tal and Metalloid Amides, Synthesis, Structures, Physical and Chemical Properties, Ellis Horwood Publishers, New York, **1980**.
[10] A. Haaland, *Angew. Chem.* **1989**, *101*, 1017–1032; *Angew. Chem. Int. Ed. Engl.* **1989**, *28*, 968.
[11] R. J. Wehmschulte, K. Ruhlandt-Senge, P. P. Power, *Inorg. Chem.* **1994**, *33*, 3205–3207.
[12] G. M. Sheldrick, W. S. Sheldrick, *J. Chem. Soc. A* **1969**, 2279–2282.
[13] K. M. Waggoner, H. Hope, P. P. Power, *Angew. Chem.* **1988**, *100*, 1765–1766; *Angew. Chem. Int. Ed. Engl.* **1988**, *27*, 1699–1705.
[14] M. A. Petrie, P. P. Power, K. Ruhlandt-Senge, *Inorg. Chem.* **1993**, *32*, 1135–41.
[15] P. J. Brothers, P. P. Power, *Adv. Organomet. Chem.* **1996**, *39*, 1–69. Particularly relevant to the present paper is the discussion of tricoordinate Al compounds with a $AlNC_2$, $AlN_{2\,C,}$ and AlN_3 core (p. 15 ff.).
[16] I. Krossing, H. Nöth, C. Tacke, M. Schmidt, H. Schwenk, *Chem. Ber.* **1997**, *130*, 1047–1052.
[17] I. Krossing, H. Nöth, B. N. Anand, *Inorg. Chem.* **1997**, *36*, 1979–1981.
[18] M. J. Frisch, G. W. Trucks, H. B. Schlegel, P. M. W. Gill, B. G. Johnson, M. A. Robb, J. R. Cheeseman, T. Keith, G. A. Petersson, J. A. Montgomery, K. Raghavachari, M. A. Al-Laham, V. G. Zakrzewski, J. V. Ortiz, J. B. Foresman, C. Y. Peng, P. Y. Ayala, W. Chen, M. W. Wong, J. L. Andres, E. S. Replogle, R. Gomperts, R. L. Martin, D. J. Fox, J. S. Binkley, D. J. Defrees, J. Baker, J. P. Stewart, M. Head-Gordon, C. Gonzalez, J. A. Pople, *Gaussian 94, Revision B.2*, Gaussian, Inc., Pittsburgh PA, **1995**.
[19] J. Mason, *Multinuclear NMR*, Plenum Press, New York and London, **1987**, 259–278.
[20] H. Lehmkuhl, *J. Organomet. Chem.* **1991**, *411*, 37–55.
[21] M. Hesse, H. Meier, B. Zeeh, *Spektroskopische Methoden in der organischen Chemie*, 4th ed., Georg Thieme Verlag, Stuttgart, New York, **1991**.
[22] R. T. Morrison, R. N. Boyd, *Lehrbuch der organischen Chemie*, 2nd ed., Verlag Chemie, Weinheim, New York, **1978**.
[23] P. C. Keller, *Inorg. Chem.* **1974**, *96*, 3073–3077.
[24] A. J. Downs (Ed.), *Chemistry of Aluminium, Gallium, Indium and Thallium*, Blackie Academic and Professional, London, **1993**, p. 3.
[25] A. Haaland, J. Hougen, H. V. Volden, G. Hanika, H. H. Karsch, *J. Organomet. Chem.* **1987**, *322*, C24.
[26] H. Nöth, *Chem. Ber.* **1983**, *116*, 3552–3557.
[27] G. Linti, R. Frey, W. Köstler, H. Urban, *Chem. Ber.* **1996**, *129*, 561–569.
[28] M. D. Healy, A. R. Barron, *Angew. Chem.* **1992**, *104*, 939–941; *Angew. Chem. Int. Ed. Engl.* **1992**, *31*, 921–928.
[29] K. Ruhlandt-Senge, P. P. Power, *Inorg. Chem.* **1991**, *30*, 2633–2637
[30] R. J. Wehmschulte, K. Ruhlandt-Senger, P. P. Power, *Inorg. Chem.* **1998**, *34*, 2593..
[31] M. Cesari, S. Cucinella, in *The Chemistry of Inorganic Homo- and Heterocycle* (Eds.: I. Haiduc, D. B. Sowerby), Academic Press, London, **1987**, vol.1, p.176–190.
[32] S. Schulz, A. Voigt, H. W. Roesky, L. Häming, R. Herbst-Irmer, *Organometallics* **1996**, *15*, 5252–5253.
[33] J. K. Ruff, *J. Am. Chem. Soc.* **1961**, *83*, 2835–2839.
[34] R. J. Wehmschulte, K. Ruhlandt-Senge, P. P. Power, *Inorg. Chem.* **1994**, *33*, 3205–3207.
[35] V. Shomaker, D. P. Stevenson, *J. Am. Chem. Soc.* **1941**, 63, 37–40.
[36] R. J. Wehmschulte. P. P. Power, *J. Am. Chem. Soc.* **1996**, *118*, 791–795.
[37] C. K. F. von Hänisch, C. Üffing, M. A. Junker, A. Ecker, B. O. Kneisel, H. G. Schnöckel, *Angew. Chem.* **1996**, *108*, 3003–3005; *Angew. Chem. Int. Ed. Engl.* **1996**, *35*, 108, 2875–2877.
[38] P. J. Brothers, R. J. Wehmschulte, M. M. Olmstead, K. Ruhlandt-Senge, S. R. Parkin, P. P. Power, *Organometallics* **1994**, *13*, 2792–2799.
[39] C. B. Lagrone, S. J. Schauer, C. J. Thomas, G. M. Gray, C. L. Watkins, L. K. Krannich, *Organometallics* **1996**, *15*, 2458–2464.
[40] A. Appel, PhD Thesis, University of Munich, **1996**; B. Wrackmeyer, U. Dörfler, M. Herberhold, *Z. Naturforsch., B* **1993**, *48*, 121–123; B. Wrackmeyer, U. Dörfler, W. Milius, M. Herberhold, *Polyhedron* **1995**, *14*, 1425-1431, 2683–2689.
[42] $Al(SiMe_3)_3{\cdot}OEt_2$, $Na[Al(SiMe_3)_4]$, $[Al(SiMe_3)_3]_2{\cdot}$tmeda, $[(Me_3Si)_2Al(NH_2)]_2$, $(Me_3Si)_3SiAl(C_6H_5)_2{\cdot}$thf, $Na[Al(SiMe_3)_4]{\cdot}2$ toluene in: M. L. Sierra, V. S. J. de Mel, J. P. Oliver, *Organometallics* **1989**, *8*, 2312–2316.
[43] G. Becker, H. M. Hartman, A. Münch, H. Riffel, *Z. Anorg. Allg. Chem.* **1985**, *530*, 29–42.
[44] A. Heine, D. Stalke, *Angew. Chem.* **1993**, *105*, 90–92; *Angew. Chem. Int. Ed. Eng.* **1993**, *32*, 121–123.
[45] H. F. Holleman, E. Wiberg, N. Wiberg, *Lehrbuch der anorganischen Chemie*, Walter de Gruyter, Berlin, New York, 101st ed., **1995**.
[46] S. J. Schauer, G. H. Robinson, *J. Coord. Chem.* **1993**, *30*, 197–214.
[47] A. Boardman, R. W. H. Small, I. J. Worall, *Inorg. Chim. Acta* **1986**, *120*, L23.
[48] S. J. Trepanier, S. Wang, *Organometallics* **1996**, *15*, 760–765.
[49] M. Veith, S. Faber, H. Wolfanger, V. Huch, *Chem. Ber.* **1996**, *129*, 381–384.
[50] I. Krossing, H. Nöth, unpublished results, publication in progress; see: I. Krossing, PhD Thesis, University of Munich, **1997**.
[51] H. W. Roesky, *Organometallics* **1997**, *16*, 1260–64.
[52] M. J. Zaworotko, J. L. Atwood, *Inorg. Chem.* **1980**, *19*, 268–271.
[53] Performed with the program: *Hyperchem*, V3.0, Autodesk, **1993**.
[54] [54a] H. Gilman, C. L. Smith, *J. Organomet. Chem.* **1968**, *14*, 91–101. – [54b] G. Gutekunst, A. G. Brook, *J. Organomet. Chem.* **1982**, *225*, 1–3. – [54c] A. Heine, R. Herbst-Irmer, G. M. Sheldrick, D. Stalke, *Inorg. Chem.* **1993**, *32*, 2694–2698.
[55] Siemens Industrial Automation, **1995**.
[56] *PC SHELXTL Rel. 5.03*, Siemens Analytical Instruments, Version 4.1, **1994**.
[57] G. M. Sheldrick, *SHELX-93*, University of Göttingen, **1993**.
[58] K. M. Waggoner, P. P. Power, R. J. Wehmschulte, K. Ruhlandt-Senge, M. M. Olmstead, M. He, M. M. Power, *Inorg. Chem.* **1993**, *32*, 2557–2564.

[97260]